12-2022

Synthesis and Characterization of VO2 Thin Films on Piezoelectric Substrates

Samee Azad
sameea@clemson.edu

SYNTHESIS AND CHARACTERIZATION OF VO_2 THIN FILMS ON PIEZOELECTRIC SUBSTRATES

A Thesis
Presented to
the Graduate School of
Clemson University

In Partial Fulfillment
of the Requirements for the Degree
Master of Science
Electrical Engineering

---

by
Samee Azad
December 2022

Accepted by:
Dr. Goutam Koley, Committee Chair
Dr. Judson Ryckman
Dr. Apparao Rao

ABSTRACT

Polycrystalline VO_2 thin films synthesized on two piezoelectric substrates (AT-cut quartz and GaN/AlGaN/GaN/Si) using low pressure direct oxidation technique have been characterized and compared to VO_2 grown on traditional non-piezoelectric substrates sapphire and SiO_2/Si. X-ray diffraction and atomic force microscopy characterization performed on the as grown films confirmed high quality of the VO_2 films grown on both the piezoelectric and non-piezoelectric substrates. Changes in material properties associated with the semiconductor metal transition (SMT) of the VO_2 films were investigated through resistivity and transmitted optical power changes measured across the SMT. It was observed that the VO_2 films grown on the piezoelectric substrates are of high quality, and their electrical and optical properties changes are quite comparable to the best reported values on films synthesized on various substrates using different synthesis processes.

ACKNOWLEDGMENTS

My gratitude goes to the Clemson University for allowing me to be one of its graduate students and providing me with a wide range of research opportunities, which I could not imagine before setting foot on this great campus. I must thank Dr. Goutam Koley from the bottom of my heart for including me into his dynamic research group and taking me under his mentorship and guidance, a rare privilege any researcher in my field would love to compete for. Since the beginning, I am always astounded by his calm and composed attitude, at the same time his zeal and passion and excitement for exploring and implementing innovative research ideas and concepts. His helpfulness towards his disciples is a great relief for us, when I get stuck in my research and start to give up hope, each time I get recharged by the inspiration and enthusiasm from Dr. Koley.

I also count myself lucky to have met and worked with Dr. Ferhat Bayram, Dr. Digangana Khan, Dr. Hongmei Li, Dr. Durga Gajula, Lavanya Muthusamy, Baaladitya Uppalapati and Makhluk Prio in our research group. My time with this great group of scientists and researchers will always be a very important part of my life and career.

TABLE OF CONTENTS

LIST OF TABLES

LIST OF FIGURES

CHAPTER ONE

INTRODUCTION TO PHASE TRANSITION MATERIALS (VO_2)

Vanadium is a metal which can forms different types of morphological structures by arranging into a wide range of coordination. A number of well-known coordination structures are: tetragonal (V_2O_4), orthorhombic (V_2O_5), monoclinic and conundrum (V_2O_6). At a lower temperature, during the semiconducting state VO_2 assumes a monoclinic structure, and at a higher temperature during the metallic state, VO_2 adopts a tetragonal (Rutile) form. In Figure 1.1 we see that, the rutile lattice form of vanadium arrangement which involves six oxygen atoms surrounding the vanadium atom. An octahedral structure is adopted by the oxygen atoms. Below transition temperature, a dimer combination of two-unit cells (vanadium - vanadium metallic bond causes the dimer along the axis) forms the monoclinic structure. A monoclinic unit cell encloses the vanadium dimer in a tilted tetragonal. The vanadium-vanadium dimer octahedron structure of oxygen gets deformed by this lopsided tilting as well.

The main reason for the VO_2 semiconductor to metal phase transition is the vanadium dimer. A combination of the vanadium atom ([Ar] $4s^2 3d^5$) orbitals and the two oxygen atoms ($1s^2 2s^2 2p^4$) forms the electronic structure of VO_2. The valence-shell four electrons from vanadium ion will complete the two oxygen atomic orbitals, leaving only one electron remain in vanadium ion. The d orbital near the Fermi level (3d) will be occupied by this electron.

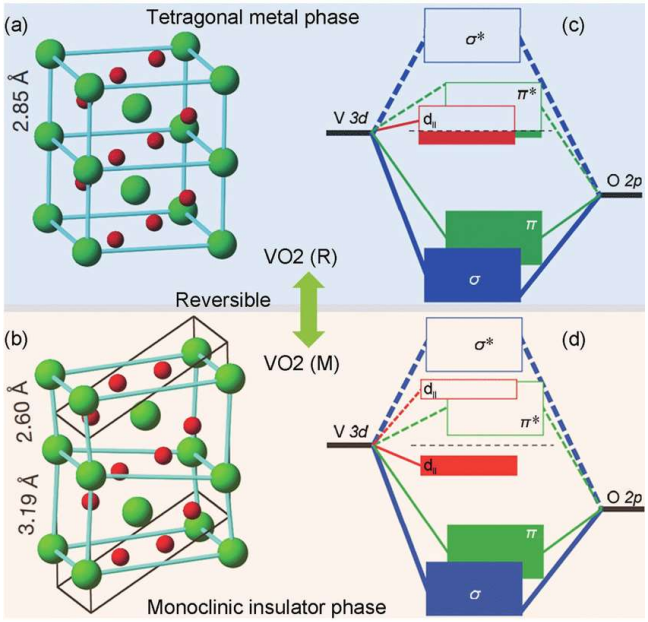

Figure 1.1: Monoclinic and rutile phases of VO_2

The electrical conductivity has no contribution from the electrons of 2p orbitals of oxygen. Since the vanadium ions have their d orbitals split into lower energy t2g and eg s orbitals because of the Fermi level being well above the electron orbital. The t2g orbital gets split into bonding (a1g) and antibonding (eg p) orbitals but since Eg s orbital is in higher energy state, it remains unoccupied. Afterwards, a1g orbital will be occupied by one electron of vanadium ion. Consequently, the bandgap of a1g and Eg p differs due to the arrangement of V-V and oxygen.

Applications and phase transition of VO_2

It was usually assumed that, an insulator and a metal have no interaction between themselves. However, when some materials reach a certain temperature or voltage, they

exhibit semiconductor to metal transition or vice versa. Since this type of materials can have good potentials for switching applications this phenomenon is highly interesting.

Semiconductor to metal transition can be triggered by various mechanisms. Such triggering mechanism may involve heating, mechanical strain, or electric fields. The properties of materials, for example, resistivity or resistance, undergo transition from semiconductor to metal and vice versa during SMT. We observed that the resistance of a VO2 thin film can change by three or four orders due to SMT, as shown in Figure 1.2. For VO2, heat triggers this transition triggered at a transition temperature typically at 67°C.

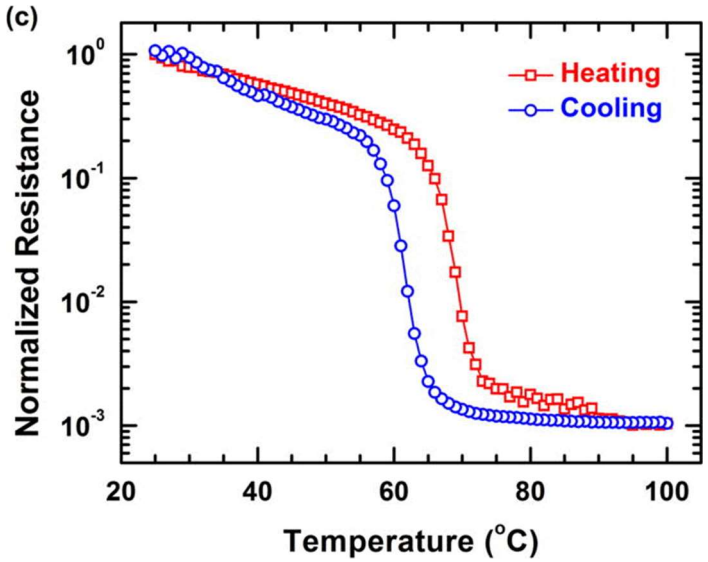

Figure 1.2: Resistance change of VO_2 due to semiconductor to metal transition

SMT can also lead to change in optical properties of the phase transition materials. We observe that in Figure 1.3 the optical transmission decrease when VO2 experiences SMT due to heating. For different wavelengths, the optical transmittance or reflectance change can be different when VO2 undergoes phase transition.

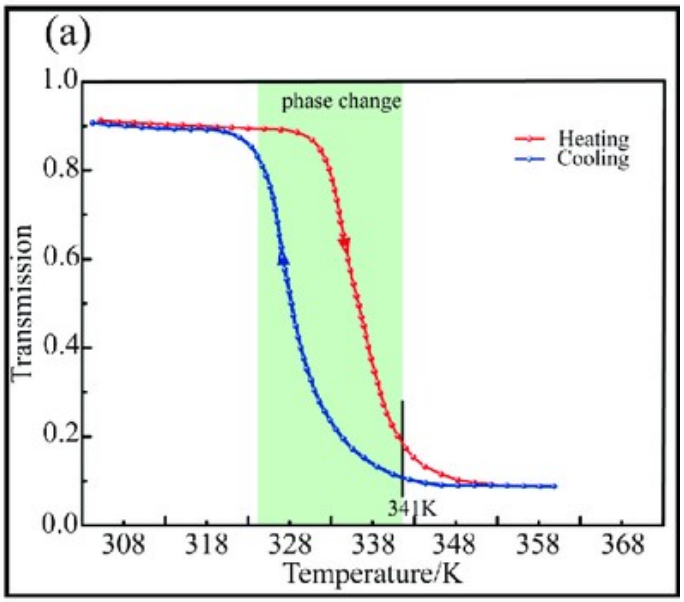

Figure 1.3: Transmitted optical power vs. temperature at 4 μm

It is still not crystal clear why and how exactly SMT occurs, even though different theories have been proposed since the last six decades. Presently, there are three theories (Mott, Peierls, Anderson) which are accepted till now. According to Mott, when a critical carrier density, nc, is surpassed by the carrier density, the electron-electron correlation comes into action. We can determine it from $n_c^{1/3}$ aH ~ 0.2 where aH is the Bohr radius of the material. It was proposed that a phase transition is initiated by this transition. There is a probability that in a lattice, conduction takes place by when electrons jump from one

site then to the immediate beside it. However, when an electron is already occupying already in the new site, the Coulomb repulsion takes place. When the electrons' kinetic energy is surpassed by the amount of repulsive energy U, the electrons cannot pass through the lattice. Due to the electrons being impeded like that, the situation initiates an arrangement of two different band groups, UHB (upper Hubbard band) and LHB (lower Hubbard band), causing the thin film to be in semiconducting state, shown in Figure 1.4. Application of adequate external factors like strain can cause the semiconducting state can shift into a metallic state.

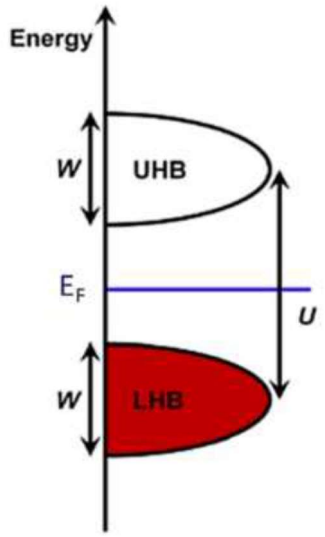

Figure 1.4: Electron correlation forms upper Hubbard band (UHB) and lower Hubbard band (LHB)

It is proposed by Peierls that when a structural change in a lattice of the material occurs, it causes the SMT. We can assume a model which involves a one-dimensional metal. Considering a lattice constant, a, and an even atomic displacement of L_0, when the

periodic chain gets distorted, a change in a repeat distance to L' occurs. Afterwards, at band opening, the new zone boundary is formed forms at π/ L', shown in Figure 1.5.

Near the Fermi level, the electrons will have lower energy considering the newly created band gap. For lattice distortion, the increase of energy due to elastic energy needs to be neutralized, which is done by the energy reduction in electrons near Fermi level, leading to transition.

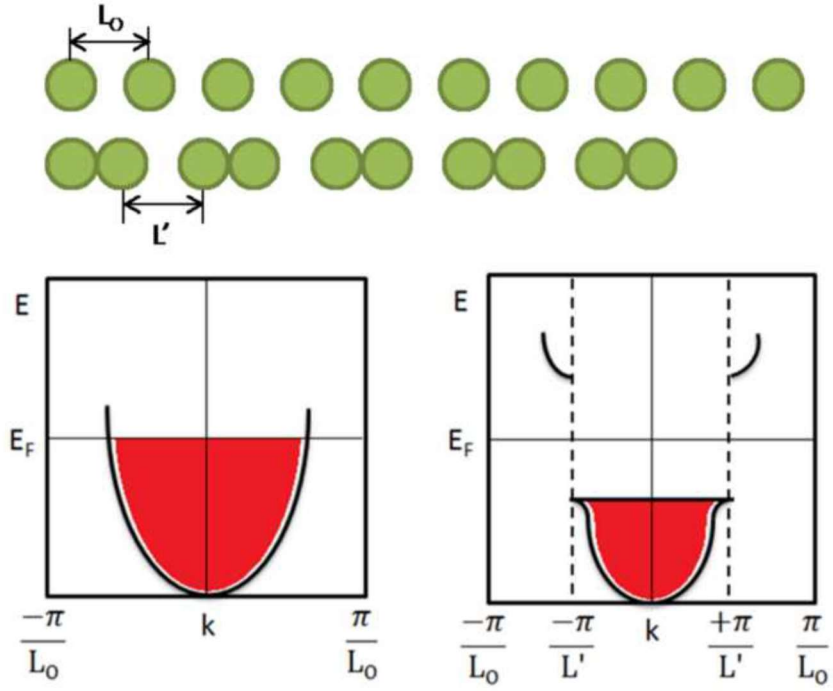

Figure 1.5: The normal lattice and the distorted lattice in a one-dimensional model, and the respective band diagrams

In the other hypothesis, Anderson utilized disorder-induced localization impact to explain semiconductor to metal transition. It is proposed that a lattice may have defects (impurities or vacancies) distributed arbitrarily, and they can scatter the conducting electrons. Non-uniform lattice potentials due to the defects in the structure can lead to localized and extended states separated.

The border between localized and extended states is characterized by the mobility edge, shown in Figure 1.6. When the Fermi energy level shifts upward or downward, the SMT occurs.

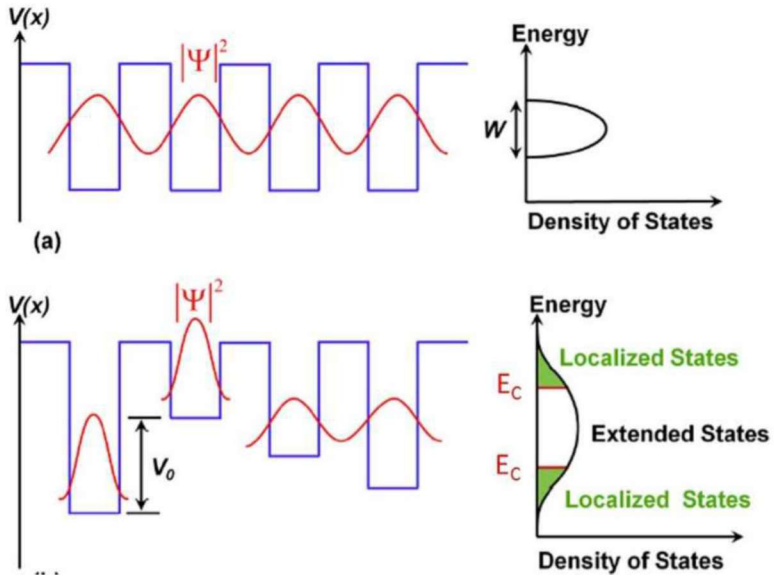

Figure 1.6: For an orderly crystal and imperfect crystal, the lattice energy and the state density

Till this time, we do not find any single decisive theory to explain the fundamental cause of SMT in vanadium dioxide. Debate is still prevalent whether the SMT is an outcome of change in structure (Peierls theory) or because of reaction of carriers (the Mott-Hubbard theory).

Vanadium dioxide (VO_2) has been a subject of extensive research in recent years because of its dramatic change in physical properties exhibited by phase transition [1]. This unique feature has spurred diverse applications in many areas including temperature and infrared (IR) sensing [2], smart windows [3], temperature based optical switch for waveguides at radio frequencies [4], and thermally switched microelectromechanical systems (MEMS) [5], as pointed out in Figure 1.8. VO_2 exists in two primary phases, a monoclinic semiconducting phase and a rutile metallic phase, and can transition from the former to the later through temperature change, application of electric field, and strain [1-3]. Although the first two methods have been commonly utilized to effect phase change, strain induced phase change has been investigated to a limited extent and only indirectly [4-5], in spite of its wide potential applications in sensing and detection, hindered in part by the difficulty in realizing devices where significant strain change can be realized. In this respect, piezoelectric substrates offer interesting possibilities of strain induced phase change simply by the application of an appropriate external electric field.

VO_2 on piezoelectric substrates

However, there are only a few existing reports on the investigation of phase transition behavior of VO_2 on piezoelectric substrates such as AT-cut quartz, or technologically interesting GaN/AlGaN/GaN/Si substrates. These substrates possess excellent piezoelectric properties, and VO_2 layers incorporated on them can be subjected to high strain through externally applied electric field or in a MEMS structure, such as a cantilever, where a VO_2 sensing element integrated at the base of the cantilever can be subjected to large deflection induced strain [6].

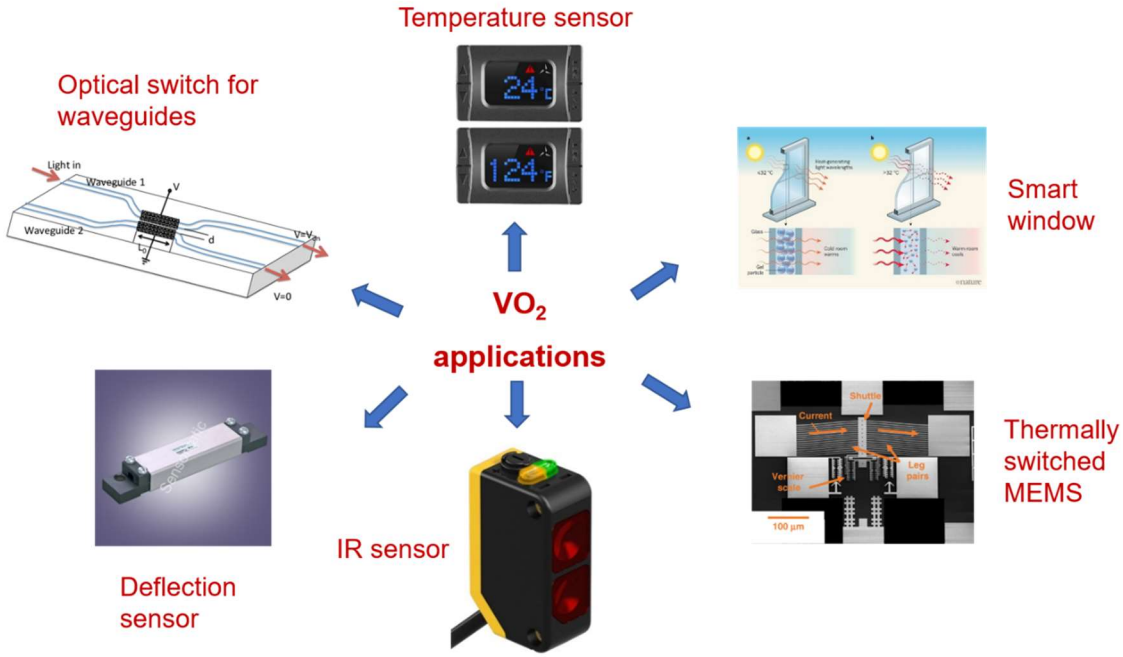

Figure 1.7: Applications of phase changing materials

Synthesis methods of VO_2 thin film

Since the very first discovery of the phase transition behavior of VO_2, researchers have been striving continuously to determine the most feasible and optimized method for synthesizing VO_2 and fabricate functional devices. Some of the synthesis methods explored include aerosol assisted chemical vapor deposition (AACVD) [7], chemical solution deposition process [8], and reactive DC magnetron sputtering [9]. In 2007, Piccirillo et al. demonstrated VO_2 deposition on glass substrate using AACVD process from vanadium (III) acetylaconate and vanadyl (IV) acetylaconate [7]. However, implementation of AACVD method resulted in a mixture of V_2O_3, VO_2 and V_2O_5, and presence of the two different oxides have been found to significantly affect the of VO_2 film characteristics. In another effort [8], VO_2 was prepared from $VOCl_2$ solution, with poly(vinylpyrrolidone), which showed good optical properties, with IR transmittance reducing by 45%, compared to the gas-phase methods of VO_2 synthesis of 41.5%. However, the vanadium precursor which is required for this method, is highly toxic [8]. The DC magnetron sputtering provides VO_2 film with a great uniformity and purity, but it requires a high temperature of 650 °C [9]. In another similar solution-based method of VO_2 synthesis VO_2 nanorods were synthesized through a hydrothermal reaction from V_2O_5 xerogel, poly (vinylpyrrolidone) and lithium perchlorate ($LiClO_4$) [10]. But it takes more than 7 days for this method to be finished, which makes it less cost effective. The atmospheric pressure chemical vapor deposition method has been applied to synthesize VO_2 on substrates like glass, SnO_2, and F-SnO_2 [11]. But the VO_2 thin films yielded from this method does not exhibit good optical properties, for example, IR transmittance change is less than 10% for lasers with near IR

wavelengths. In another report V_2O_5 was prepared by sol-gel method on fused-quartz substrates and pure polycrystalline VO_2 was synthesized by annealing V_2O_5 at 550°C for 10 hours, which performs great, but the method is highly expensive and time consuming [12]. The pulsed laser deposition (PLD) technique has gained popularity more recently due their ease of synthesis of VO_2 on various substrates, including sapphire and Si [13]. However, this method resulted in VO_2 films with weak modulation in transmittance characteristics 2.3%, 5.4%, 4.8%, and 2.2% for different wavelengths 400 nm, 500 nm, 600 nm and 700 nm, respectively [13].

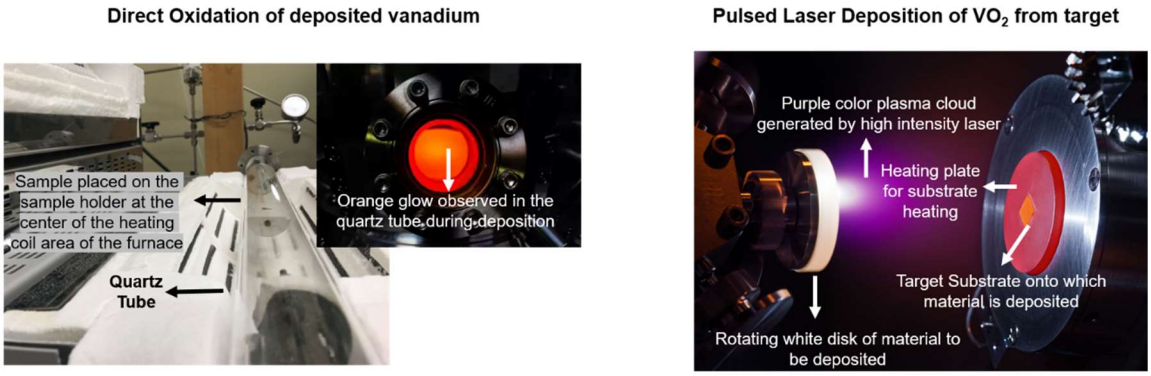

Figure 1.8: Comparison of VO_2 synthesis techniques

Some good quality VO_2 film synthesized on silicon and quartz substrates using chemical vapor deposition (CVD) technique, with Vanadium acetylacetonate as precursor has also been reported [14]. The problem is the room temperature resistances of the thin films grown from this method at 400 – 450 °C, which are in kilo ohm range only, making the VO_2 less semiconducting than it should be [14]. Reactive high-power impulse magnetron sputtering is also an attractive technique for VO_2 film deposition, where the

chamber temperature is only 300 °C only, and it yields good change of electrical resistivity by 350 times and good optical transmission variation [15–18].

VO_2 synthesis by direct oxidation

In addition to the aforementioned techniques, research efforts have been focused on direct oxidation of deposited Vanadium film, which is attractive due to its simplicity and inexpensive process, resulting in large area high quality VO_2 films on a large variety of substrates of varied shape and topography [19, 20]. Additionally, VO_2 patterned growth can be achieved by simply patterning the deposited vanadium metal. The direct oxidation method of VO_2 synthesis has been extensively studied on films grown on sapphire, where high quality films, comparable to those deposited by PLD technique has been observed [19–21]. In this work, we have investigated the structural, electrical and optical phase transition properties of VO_2 thin films synthesized using direct oxidation method on two piezoelectric substrates, AT-cut quartz and GaN (2 nm)/AlGaN (18 nm, 25% Al)/GaN (1.8 μm)/Si, and compared with those grown on two traditional substrates sapphire and SiO_2 (100 nm)/Si. The properties of the films grown on piezoelectric substrates were found to be quite comparable, and sometimes superior to those grown on the traditional substrates, which is highly promising for various sensing, actuating and optical modulation applications and synthesis parameters.

Semiconductor to metal substances have a wide range of applications. The reason is that SMT materials have a great capability to adapt and adjust structural and electrical property at a considerably short time frame. By utilizing these abilities, we can achieve a system which can provide switching robustly and inexpensively. For example, a high-speed noise signal can destroy an electric-electronic system if its voltage amplitude level is more than the acceptable threshold. To solve this type of issues, the systems can be protected by the SMT materials which changes their phase when triggered by the excessive voltage level allow the noise signal to pass through alternative circuit paths within a very short time duration. It is one of the fundamental properties of VO_2 which involves resistance increase or decrease abruptly at below or above a threshold voltage. This controlling of threshold voltage is a necessity; therefore, we can change this voltage by metal-doping or geometric changes in the thin film surface. Thus we can 'edit' the crucial voltage required to allow the extra voltage noise to pass through alternative paths. This type of application is common in electric and electronic appliances being used every day.

In the current era of widespread use of lithium ion batteries, the phase transition materials like VO_2 can play a great role here. Recently, the Li-ion batteries are being used widely in electric vehicles. Till now this is the best type of battery to replace fuel in the EVs, but the most hazardous issue is the explosive nature of Li-ion batteries. Positive Temperature Coefficient of Resistance (PTCR) is a device used in batteries to protect the circuit from being destroyed by short-circuit or overcurrent. It can impede the extra current flow when it senses the overheating in the battery. At this heated condition, the blocked

electrons face instability and causes the battery pressure to rise internally, leading to explosion.

In this type of scenarios, an SMT material like VO_2 can be a savior to protect the users from battery explosion, which can lead to severe injuries, even death. If we use SMT material like VO_2 as a part of the explosion protection, the material will shift from semiconducting to metallic at overheating conditions. At conductive state like this, the battery will discharge quickly before there occurs any risk of explosion.

Thermochromic windows are one of the researches which involves phase transition materials extensively. We know that optical transmittance through VO_2 film reduces at infrared region, because of the VO_2 becoming metallic at high temperature and reflecting off the incident optical beam and reducing transmission.

That is why, during the cool weather, the VO_2 coating on the window glass remains in semiconducting or insulating phase, and allows both light and heat to pass through to keep the indoor environment warm naturally. During hotter weather, when the VO_2 coating undergoes SMT above critical temperature, it becomes metallic, and reflects off the heat (IR wave), thus keeping indoor cooler.

Another important characteristic is when VO_2 undergoes SMT and changes into metallic state at temperature above the critical threshold, it can reflect off the infrared

waves (heat) and allows the shorter wavelength light (visible range) to pass through itself. The wavelengths of visible light can transmit through almost at the same rate, allowing no disruption of incoming light into the indoor.

CHAPTER TWO

SYNTHESIS AND CHARACTERIZATION TECHNIQUES OF VO_2 THIN FILM

For synthesis of VO_2 thin film, a good number of techniques have been developed and implemented such as Pulsed Laser Deposition, Sputtering, Chemical Vapor Deposition, Direct Oxidation and many more. In our laboratory, we have prioritized a few criteria to select the most feasible growth method. The cost has to be low, and the crystalline quality should be high enough according to laboratory standard. Among the techniques, the following two are quite notable; Pulsed laser Deposition and Direct Oxidation. These two are chosen because of their high probability to synthesize good quality of VO2 thin film in laboratory environment. These methods have different features. For our research we selected the direct oxidation considering the availability of our budget, equipment and post-synthesis processing of the thin film.

Pulsed laser deposition:

One of the notable physical vapor deposition techniques is pulsed laser deposition (PLD). Its applications are quite diverse, and frequently required for optical coating, semiconductor coating and industrial coating, metal sputtering and so on. Also it is required for dielectric coating. Dielectric coatings are non-conducting insulating materials which gets charged. In a plasma region Reactive Sputtering most frequently uses Pulsed Laser Deposition. The chemical reaction takes place between the vaporized target material and oxygen in an ionized form. Silicon oxides and other molecules get structured by this chemical reaction. Some insulating materials like titania, silica and

alumina are impossible to deposit with straight DC sputtering. In those situation, pulsed laser deposition comes to rescue with reactive sputtering. Pulsed laser deposition can provide better deposition rates than RF sputtering for thin films at feasible pulsing periods. Consequently, the quality controlled issue is resolved which occurs due to arcing.

Direct oxidation:

Direct oxidation involves oxidizing a material previously deposited on a substrate. Direct oxidation combines oxygen with other gases in a process chamber made from quartz at an optimum temperature and pressure. The oxygen mixed gaseous reactants flows inside the chamber in a laminar way, and reacts with the heated substrate placed inside the chamber. A material film is created on the substrate surface by the mixture of oxygen and other gases. At the same time, a vacuum pump pulls out the waste gases from the quartz chamber. For the reaction to take place, the substrate has to be heated up to the crucial temperature and the temperature has to maintained consistently throughout the oxidation process. Therefore, for a decent quality of direct oxidation, the correct temperature has to be chosen, because it is directly related with the material quality. The direct oxidation process creates a thin film coating of oxide on the substrate at a medium rate. Direct oxidation and physical vapor deposition (PVD) are almost similar in some ways. In PVD, solid materials are vaporized and reacts and creates the coating on substrate, and direct oxidation involves reactants which are gaseous and solid in the first place and never vaporized. Direct oxidation is advantageous in the sense that it can

synthesize high quality pure and water-resistant material on the substrate. It, through these advantages and cost effectiveness (for the film quality deposited) over other methods, is one of the most sought-after thin film deposition method in the semiconductor industry and optoelectronics. After the direct oxidation, the final product can be a bulk or thin film or thick coating, any of them can be of monocrystalline, polycrystalline and amorphous structure. The synthesis and structure of the ultimate oxidized product are dependent upon the physical parameters and chemical ingredients selected for the reaction. In the field of solid-state electronics, this method has become one of the most crucial growth techniques of depositing thin films and coatings. Direct oxidation technique is one of the branch methods of the umbrella technique chemical vapor deposition (CVD), which also involves reduction, nitride formation, carbide formation and hydrolysis. A sequence of various reactions is customarily involved in creating a unique product. The reactions might be heterogeneous, or homogeneous reaction. Reactions of heterogeneous type are a preferable because of slower rate of reaction between gaseous components and solid substrate, ensuring uniformity of the deposited film. Homogeneous reactions cause outliers and unwanted clusters in the deposited film, making it non-uniform, that is why it is not preferable.

Synthesis of VO_2

VO_2 films were investigated in this work were synthesized using a homemade low pressure furnace (Figure 2.1) through controlled oxidation of vanadium thin films of desired thicknesses deposited on the substrate of choice (c-plane sapphire, SiO_2/Si (100),

AT-cut quartz, or GaN/AlGaN/GaN [c-plane or (0001) plane])/Si (111) using electron-beam evaporation with a deposition rate of 1.5 A°/s. Prior to growth diced substrates with nominal dimensions of 1 × 1 cm, pre-deposited with a thin film of vanadium (using vanadium pellets from Kurt J. Lesker Inc. with 99.7% purity), were thoroughly cleaned using standard cleaning procedure to remove the grease and unwanted debris from the surface, before loading into the furnace chamber. Once the chamber pressure may reach 4.53 Pa under pump down, N_2 gas (purity 99.999% from Airgas) flow was started at a constant rate of 400 sccm until the chamber pressure stabilized at ~2666 Pa. The temperature of the furnace was then increased to 475 °C, and O_2 flow started at the rate of 100 sccm. The optimized growth conditions for VO_2 films (starting with 70 nm Vanadium deposition, nominally targeting 140 nm VO_2 thickness, following the Deal-Grove model) on the various substrates are summarized in Table 1.1. The oxidation durations were optimized over several growth iterations to ensure high quality of the VO_2 films, carefully avoiding under-oxidation and over-oxidation. It can be seen from Table 1.1 that the growth duration for optimized VO_2 growth on AT-cut quartz substrate was slightly longer than for other substrates (inadequate growth duration resulted in incomplete oxidation of the Vanadium film). We are not sure of the cause for such a long growth duration, but it clearly indicates the strong role of substrate on the synthesis process.

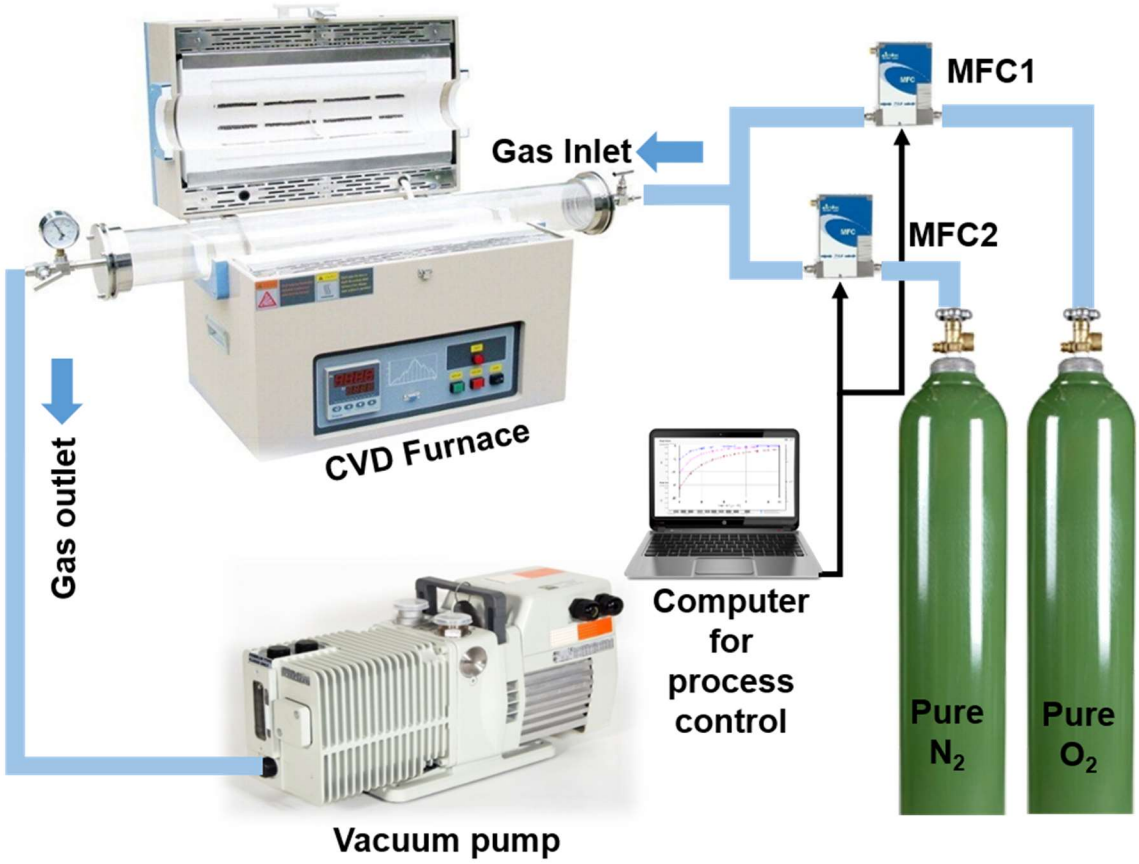

Figure 2.1: The experimental set up for direct oxidation based VO_2 synthesis used in this study

Characterization Techniques of VO_2

Following synthesis, the VO_2 thin films were characterized using optical microscopy captured using microscope Olympus BX41M-LED at 50× magnification and atomic force microscopy (AFM, Veeco Dimension 3100) operated in tapping mode and processing the data using the AFM software application of the apparatus. To determine the lattice structure and purity of the VO_2 film, X-ray diffraction (XRD) measurements (Rigaku Ultima IV system) were made on the VO_2 samples grown on the four substrates,

using Cu Kα radiation (wavelength 15.406 nm) where the diffracted beam was recorded from 5° to 90° with a step size of 0.02°. X-ray diffraction is a robust and excellent method to characterize solids of different types of crystalline structure, which has an infinite length of series of unit cells. Incident light gets diffracted by a series of 3D arrangement of particles, according to Bragg.

Table 2.1: Summary of the optimized material synthesis parameters for VO2 samples grown on four different substrates Sapphire, SiO2/Si, AT-cut quartz, and GaN/AlGaN/GaN/Si

Substrate	**Optimized VO_2 Growth Parameters**			
	Temperature (°C)	**Pressure (Pa)**	**Oxidation time (min)**	**Vanadium thickness (nm)**
c-plane Sapphire	475°	5.2	50	70
SiO_2/Si	475°	6	40	70
AT-cut Quartz	475°	7.5	70	70
GaN/AlGaN/GaN/Si	475°	4.5	60	70

The phenomenon can be explained by the equation, $n\lambda = 2d \sin\theta$ (Bragg's Law) where λ = light wavelength, Cu Kα radiation (wavelength 15.406 nm) here, d = spacing between the planes of the 3D crystal, θ stands for the angle between incident light and the

planes of the crystal (parallel). Constructive interference takes place when the atoms and their electrons scatter the incident x-ray and we plot the data as peak intensity vs. 2θ. Patterns show peaks of different intensities at certain angles of 2θ, which are like 'signatures' of particular phases in a plane of the crystal. Lattice size and centering determines the values of inter-planar distance d. X-ray absorption and diffraction by the atoms in the crystal determine the intensities of the characteristic peaks.

The solid sample, it may be crystalline or amorphous, is placed as a target for the source of x-ray. The d-spacing and the lattice of the crystal play the role for diffracting the x-ray beam incident from the source. The intensities are determined from the diffracted beam, providing the powder pattern These diffracted rays are measured at certain angles to view intensity. Ultimately the XRD pattern is plotted with peak intensity vs. 2θ. In order to recognize an existing phase, the XRD pattern and the inter-planar distances are used to search through the XRD database.

Electrical resistivity changes over the range of semiconductor metal transition (SMT) in the VO_2 thin films (effected by varying the sample temperature from 20 to 120 °C) were measured using a setup as shown in Fig. 2.1. The inset shows two probes contacting the surface of the VO_2 thin film for resistance measurement, which were connected to a Datalogger (Keysight 34972A LXI Data Acquisition Unit). An annular ceramic heater (positioned below the sample in direct contact with it) is also shown in the inset, which was used to heat the sample over the desired measurement temperature

range. A thermocouple was also placed on the VO_2 sample, to ensure accurate measurement of sample temperature simultaneously with the measurement of the substrate resistivity changes.

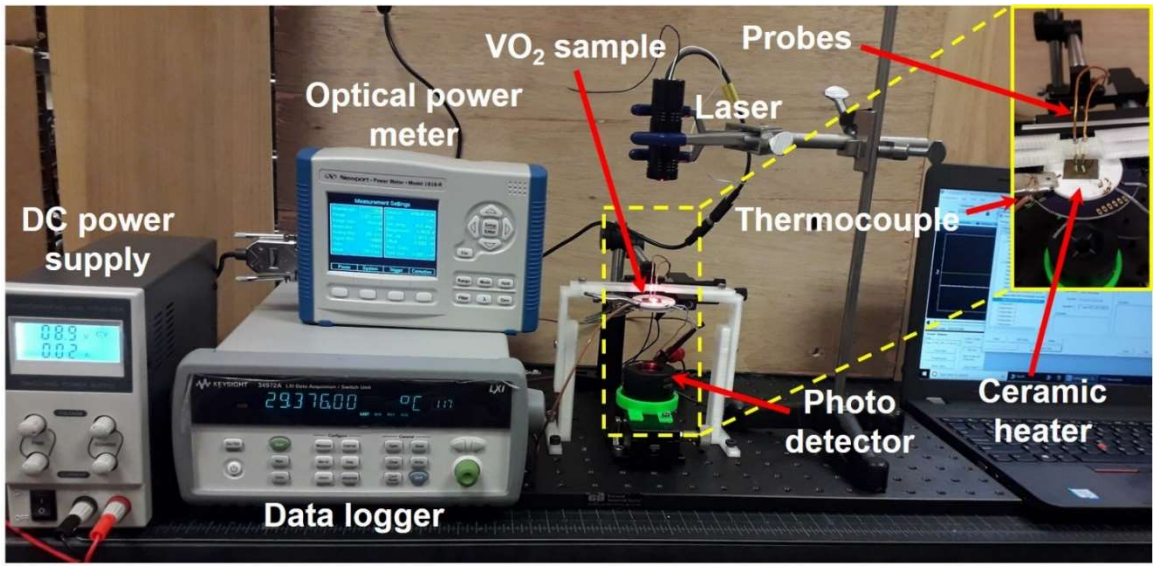

Figure 2.2: Experimental setup for electrical and optical characterizations of the VO_2 thin films. The laser is shone from the top, while a photodetector at the bottom (along with a power meter) measures the transmitted laser power as phase transition occurs. Inset shows magnified image of the white annular ceramic heater with the sample on top contacted by two current measurement probes.

In addition to the electrical characterization, variation in transmitted optical power (for transparent films) with temperature is often investigated to determine optical property changes associated with SMT. Transmitted optical power through VO_2 thin films undergoes a sharp transition during SMT, which is significantly higher for infrared light compared to visible light. Like the resistivity change, the transmitted optical power was also measured spanning across the SMT for the VO_2 thin films as a function of temperature, using the same characterization setup as shown in Fig. 2.1. An IR laser was held with a clamper above the sample at an optimal height so that the laser is focused on

the sample, while a photodetector (Newport 918D-IR-003R, range 780 to 1800 nm) was placed beneath the central hole of the annular ceramic heater to measure the transmitted light power, with the help of a Newport 1918-R power meter.

CHAPTER THREE

RESULTS AND DISCUSSIONS

Material characterization

Figure 3.1 shows the optical microscopic images of the VO_2 samples grown on the four substrates, i.e., sapphire, SiO_2/Si, quartz and GaN/AlGaN/GaN/Si while surface morphology images (5 × 2.5 μm) and the root-mean-square (rms) surface roughness of the polycrystalline VO_2 samples synthesized on the various substrates are shown in Fig. 4.

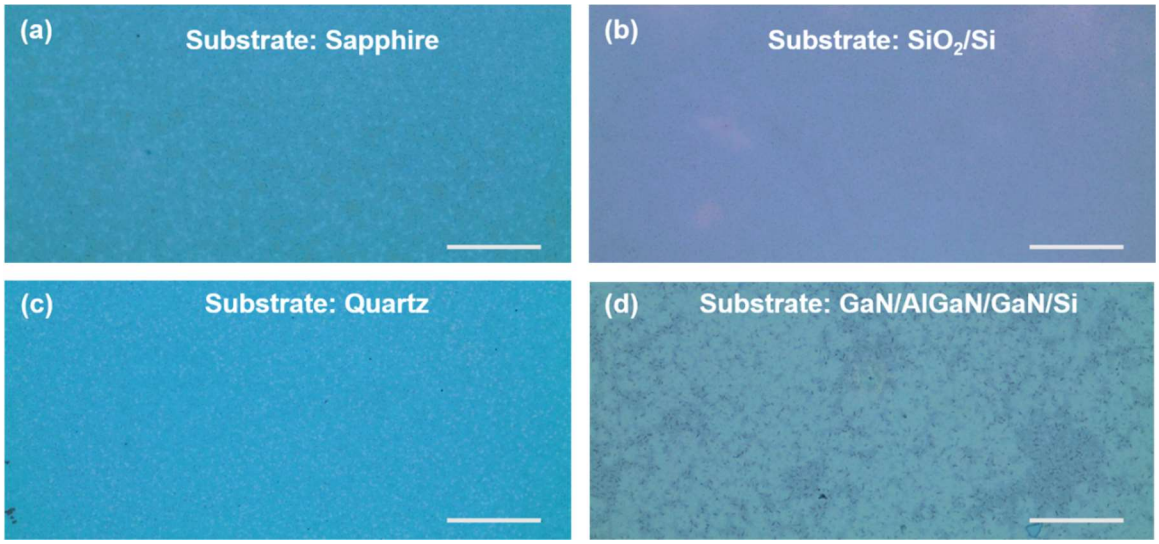

Figure 3.1: Optical images (50× magnification) of VO_2 thin films (5 mm × 3 mm) synthesized from 70 nm Vanadium deposited on (a) c-plane sapphire, (b) SiO_2/Si, (c) AT-cut quartz, and (d) GaN/AlGaN/GaN/Si substrates. The scale bar: 500 μm for all substrates

From Fig. 3.1, we find the films to be mostly uniform with some granularity, as expected for the polycrystalline thin film layers. The bluish-green and purple color of VO_2, in comparison with what mentioned in literature [22], is also clearly noticeable in all four images shown in Fig. 3.1.

For analyzing the surface topography of thin films with precision and resolution range down to nanometer level, the Atomic Force Microscope (AFM) is used for that purpose. AFM components include, a tip with cantilever the scanning unit, the optical measurement unit including the laser and the camera, and the electronic circuitry for handling the feedback signal. The tip scans the sample surface with the cantilever in a series of lines, restarts the scanning along a new line after reaching the end of its previous line. The topography of the thin film is measured by the interaction between the tip and the thin film surface., but also other properties can be measured by analyzing the tip-sample interaction (e.g. variations in local stiffness, friction force and lateral stiffness).

The probe position is controlled by a high precision scanner, which can be maneuvered in all three dimensional directions (X, Y, Z). The surface topography of the film causes the cantilever to be deflected and the intra-planar friction causes twisting around its horizontal axis during scanning in the lateral orientation. An optical detection system including a photodetector is used to measure the cantilever deflections. The other side of the cantilever reflects off a laser beam incident on it and the reflected beam gets detected by the photodetector. Four quadrants form the photodetector and the bending signals of the cantilevers are measured by differentiating the optical powers between either the right and left halves, or the lower and upper halves. Ultimately, we use this equation to normalize the difference of the optical power:

$e = (A + D) - (B + C) / (A + B + C + D)$

$f = (A + B) - (C + D)/ (A + B + C + D)$

In Fig. 3.2, the AFM images are displayed. The rms roughness values were calculated as 8.19, 7.37, 10.3 and 9.75 nm for VO_2 samples grown on sapphire, SiO_2/Si, quartz, and GaN/AlGaN/GaN/Si, respectively (Table 3.1). The uniformity of the roughness numbers indicates consistent morphological quality of the VO_2 thin films, which compare favorably with the surface roughness values reported in the literature, as expected from a polycrystalline film of monoclinic grain structure [19], typically, an increase in surface roughness in films is observed with an increase in oxidation time, as reported by Lindstrom *et al.*, where the VO_2 surface roughness was found to increase from 35 nm to 60 nm when the oxidation time was increased from 5 to 90 minutes [23].

Fig. 3.3 show the typical X-ray scans, in which the characteristic peaks for VO_2 films synthesized on c-plane sapphire are found at 38.36° for VO_2 (020), and 44.6° for (012), with VO_2 (020) being the prominent peak [24]. For SiO_2/Si, obvious VO_2 peaks are found at 38.42° for (020) plane, 44.66° for (012) plane, and 69.28° for (202), the most prominent one.

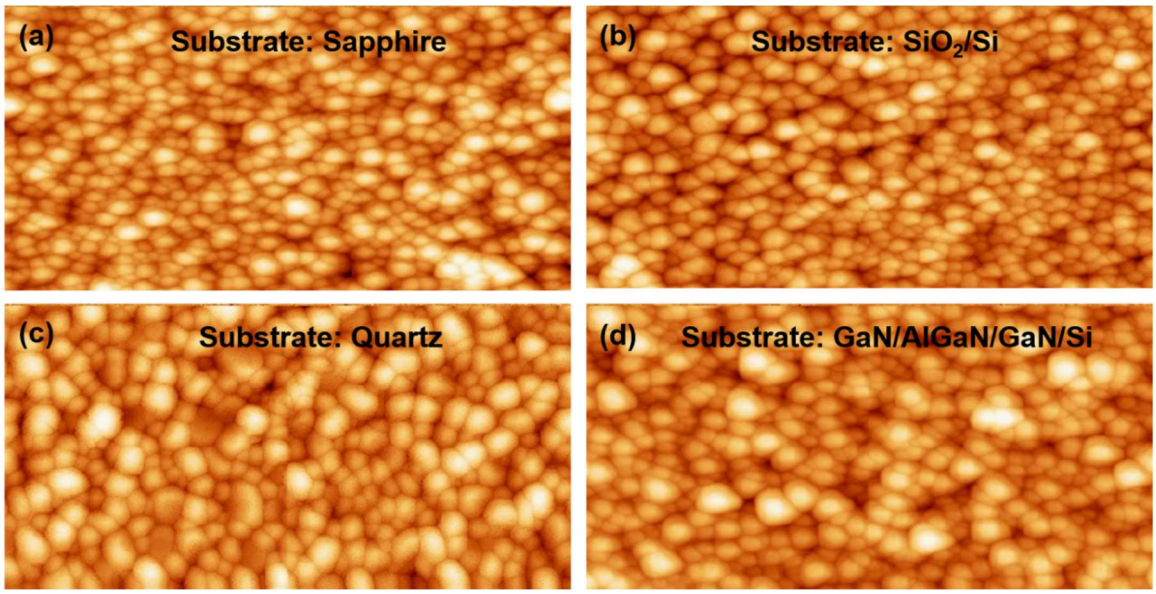

Figure 3.2: Surface morphology images (5 × 2.5 μm) of thin films synthesized from 70 nm Vanadium deposited on (a) c-plane sapphire (z-scale bar 58.1 nm), (b) SiO_2/Si (z-scale bar 50.4 nm) (c) AT-cut quartz (z-scale bar 75.4 nm), and (d) GaN/AlGaN/GaN/Si (z-scale bar 68.1 nm) substrates.

For VO_2 on quartz, conspicuous peaks are exhibited at 38.5° (the prominent peak, 020 plane), and 44.74°, for (012) plane. For GaN/AlGaN/GaN/Si (111), we see VO_2 intense diffraction peaks at 38.52° for (020) and 44.76° for (012) plane, which are quite comparable to those reported in the literature (JCPDS card no. 44-0252) on various substrates [24–26]. For all four substrates, the common intense diffraction peak exists for VO_2 (020), prominent in all four except for SiO_2/Si substrate. For sapphire, SiO_2/Si, quartz and GaN/AlGaN/GaN/Si, VO_2 (020) is found at 38.36°, 38.42°, 38.5° and 38.52°. A summary of the 2θ peak position and the full width at half maximum (FWHM) values for the prominent peaks are presented are summarized in Table 3.1, where the tight range of the FWHM (0.06° – 0.20°) indicate high directionality of the polycrystalline domains in the VO_2 films.

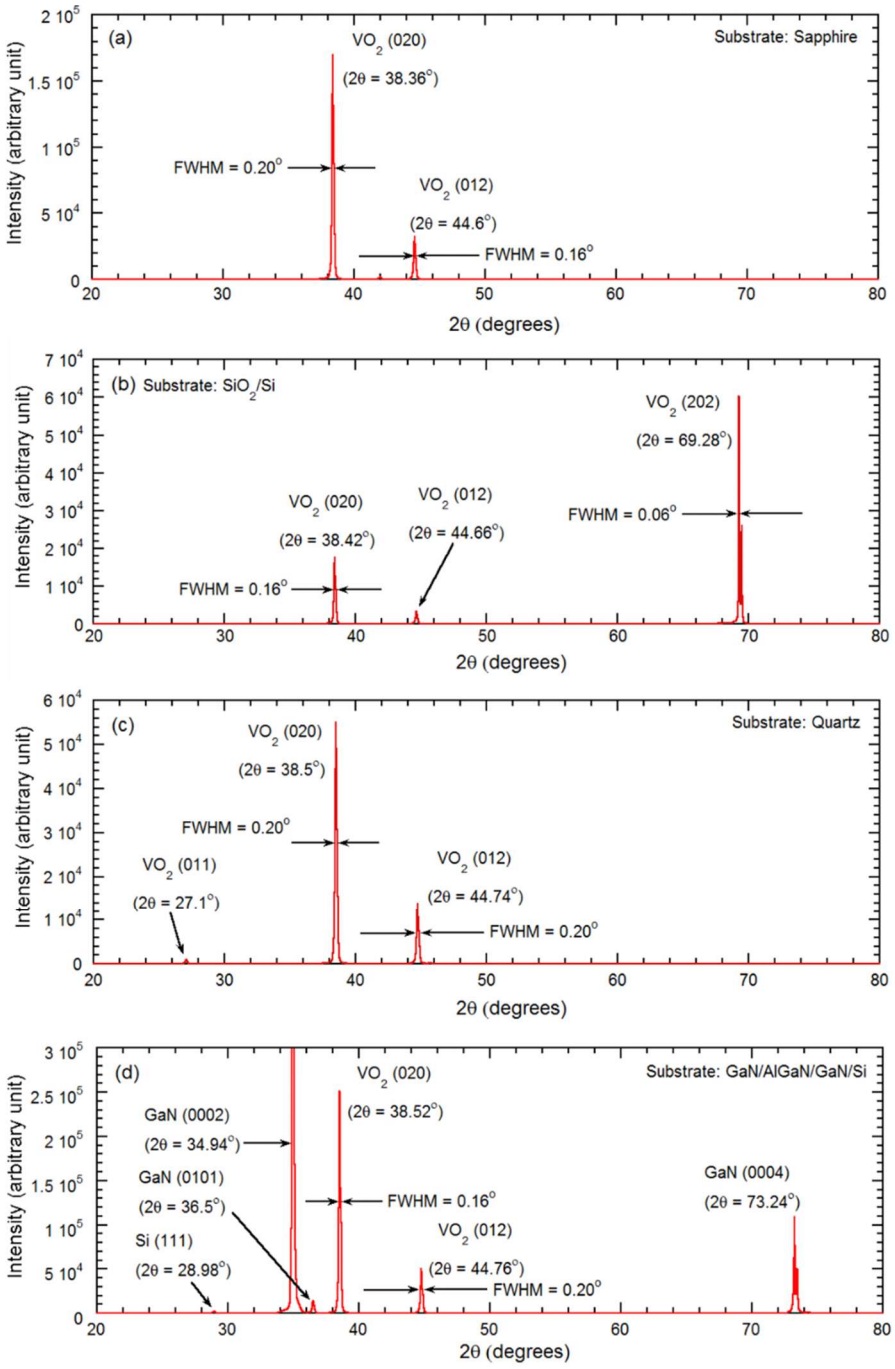

Figure 3.3: X-ray diffraction peaks are presented for the VO_2 thin films synthesized on (a) c-plane sapphire, (b) SiO_2/Si, (c) AT-cut quartz, and (d) GaN/AlGaN/GaN/Si substrates. The VO_2 (020) and VO_2 (012) peaks, along with their respective full width at half maxima (FWHM), are pointed out with arrows.

Electrical Characterization

Fig. 3.4 shows the change in resistivity, both in forward and reverse directions, of typical VO_2 films on all four substrates when their temperature was varied from 20 to 120 °C. The average transition temperature (from the forward and reverse characteristics), determined to be the point of maximum slope of the respective transition curves, were found to vary within a narrow range among the substrates, with the maximum T_c of 72 °C recorded for VO_2 on SiO_2/Si substrate, and the minimum of 61 °C for VO_2 on quartz substrate. The T_c values, temperature ranges of transition (taken as $T_c \pm 20$ °C), and resistivity ratios (corresponding to the lower and upper SMT of the temperature range) for all four substrates are summarized in Table 3.1. The highest transition ratio of 1094 was recorded for VO_2 on sapphire, while the lowest of 665 was observed for the film grown on GaN/AlGaN/GaN/Si substrate. Although the VO_2 films on piezoelectric substrates, GaN/AlGaN/GaN/Si and AT-cut quartz, exhibited somewhat lower transition resistivity ratios compared to those of the traditional substrates, sapphire and SiO_2, still those ratios are quite significant for practical usage of those films.

The slope in the electrical resistivity curve before and after SMT are typically attributed to hopping transport of the carriers through Frenkel-Poole mechanism [27]. The activation energy of the carriers can be determined from the Arrhenius plots corresponding to the relevant sections [28–33].

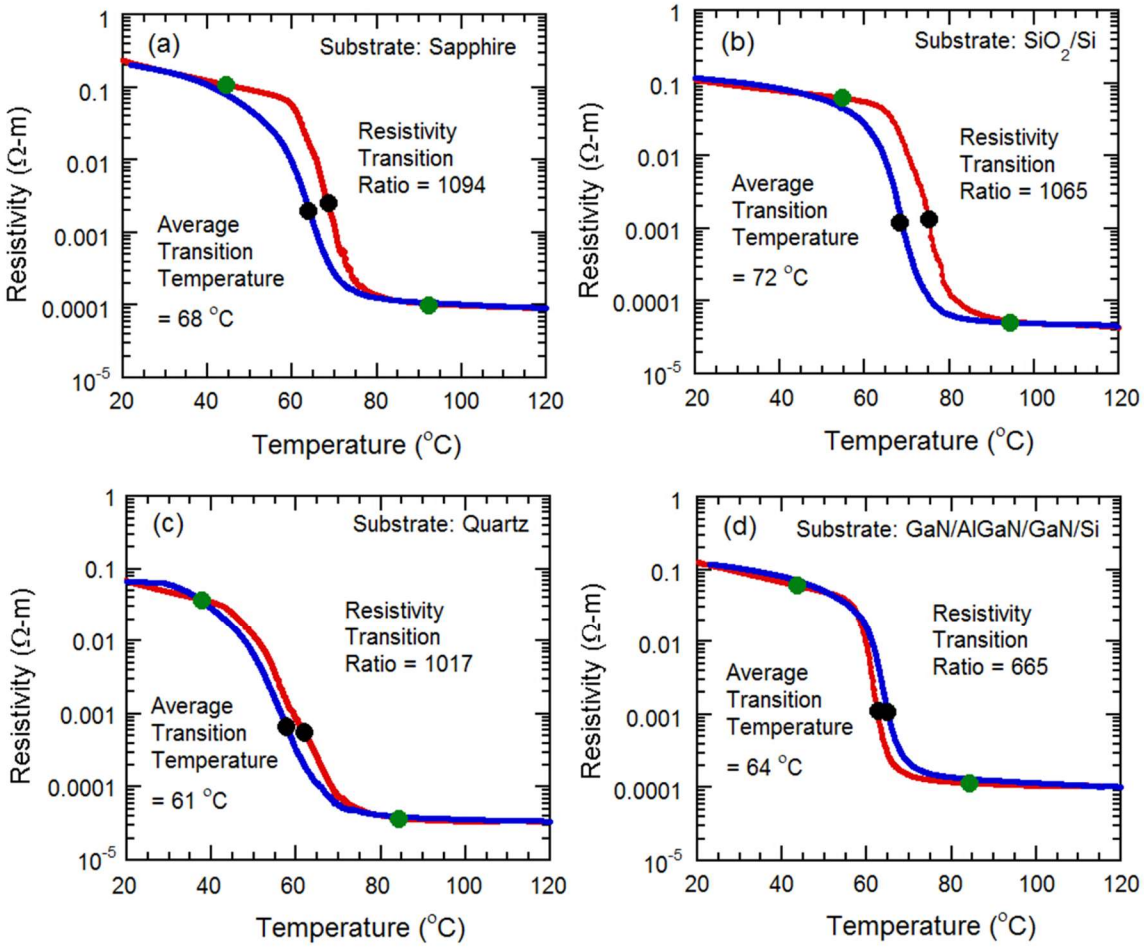

Figure 3.4: Semi-log plots of resistivity variation as a function of temperature for the VO_2 thin films grown on various substrates as they undergo semiconductor-metal transition (SMT). The transition resistance ratios, along with the beginning (green dots), mid (black dots, corresponding to maximum slope points in the curves), and end transition temperatures (green dots) are shown for all the samples

The Arrhenius equation correlating the VO_2 film resistance R (for relevant sections) and the activation energy E_a is given as: $R = Ce^{-\frac{E_a}{kT}}$, where k is Boltzmann constant, and T is the absolute temperature. By taking natural logarithm of both sides, the equation can be written as: $\ln(R) = -\frac{E_a}{kT} + \ln(C)$, which allows the activation to be determined directly from the slope. Figures 3.5 (a) – (d) shows plots of ln(R) vs. (-1/kT) for the VO_2 films on all the substrates, utilizing the electrical characterization results

shown in Fig. 3.4. For each film, the semiconducting and the metallic sections (before and after SMT, respectively) of the plots have been fitted with straight lines, and the corresponding slopes have been noted to determine the activation energies. The activation energies for the VO_2 thin films on all four substrates have been recorded in Table 2.1, for both semiconducting phase and metallic phases. The activation energies found from the Arrhenius plots were found to vary from 0.06 – 0.3 eV), which is consistent with the values reported in the literature [34–36]. As we can see from Table 3.1, the activation energies are found to be significantly lower (by a factor of ~5) for metallic phases (at higher temperature), which is expected and indicates that less energy is required by the carriers to overcome the threshold energy barrier for conduction.

We would like to point out here that the synthesis of VO_2 on III-Nitride epitaxial layers was only once reported earlier, by our group [35]. In the previous report from our group a transition ratio of ~300 was recorded on GaN/AlGaN/GaN/Si substrate with a T_C of 65 °C. The transition ratio of ~ 665, reported here in this paper is clearly a significant improvement over that, and the transition temperature is also found to be 64 °C, which is comparable to that reported earlier [35]. While further investigation is necessary for further understanding of the impact of strain and substrate in the VO_2 films, our results clearly indicate a great promise for developing highly sensitive MEMS devices using these films, when used in conjunction with the piezoelectric III-Nitride films [6, 35–39] and quartz [40]. Comparison with other reports are shown in Table 3.2.

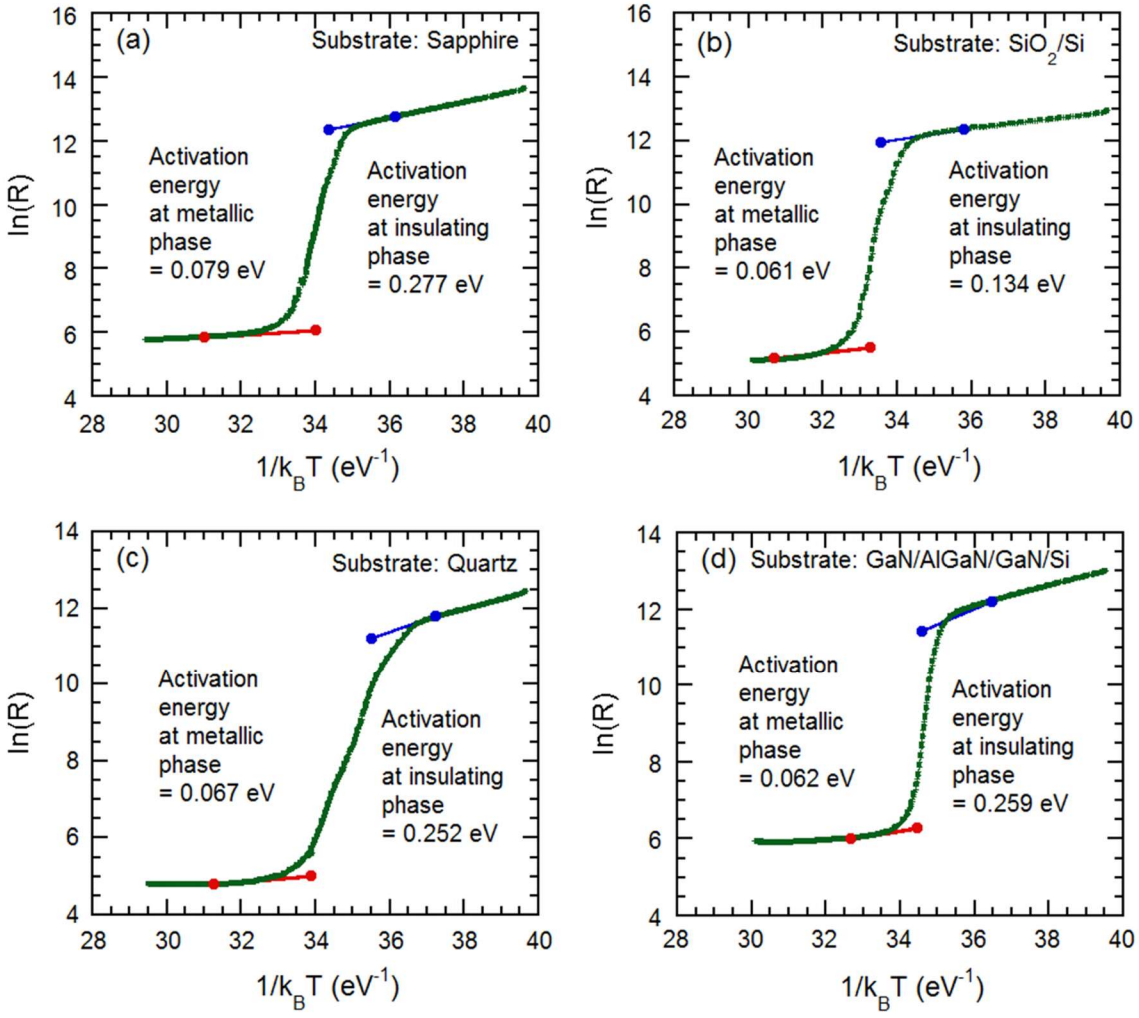

Figure 3.5: Arrhenius plots (green curves) for the VO_2 films synthesized on the different substrates. The blue and red lines are linear fits to the relevant sections of the semiconducting (pre-SMT) and metallic (post-SMT) phase plots, respectively. From the slopes of the linear fits, the activation energies corresponding to the particular phases have been determined and include in the figures.

Optical Characterization

Figures 3.6 (a) – (d) show the experimental results on the variation of transmitted optical power through the VO_2 films grown on AT-cut quartz and c-plane sapphire for two IR lasers wavelengths 980 and 1064 nm. A sharp change in transmitted laser power

through the VO_2 thin film is observed at SMT, as expected, since semiconducting VO_2 allows IR light to transmit through it before SMT, while "metallic" VO_2 film resulting after SMT, acts as a lossy medium for the electromagnetic (EM) waves [41], and causes a sharp drop in the transmitted power. A reduction in transmitted laser power by 46.2% at 980 nm, and 54.8 % at 1064 nm, was observed for the VO_2 film on sapphire substrate, whereas for the film on AT-cut quartz substrate, the transmitted laser power decreased by 45.6% at 980 nm, and 55.8% at 1064 nm. A summary of the optical properties of the films are presented in Table 3.1. We note that the change in transmitted optical for sapphire and quartz are one of the highest reported so far at 1064 nm. We also note that the actual magnitude of the transmitted power for both the substrates is much lower for 980 nm compared to 1064 nm, since the optical transmittance changes much more drastically as the wavelength increases [42]. We also note here that the forward optical transitions are much sharper compared to the reverse transitions. This has been observed to some extent for the electrical characteristics as well, but not as prominently as seen for the optical ones. This "lag" may be due to the slower rate of cooling of the region exposed to the laser, when the substrate is cooled, as the optical absorption in the highly conductive material (the area where laser is focused) is high, preventing quick changes in temperature.

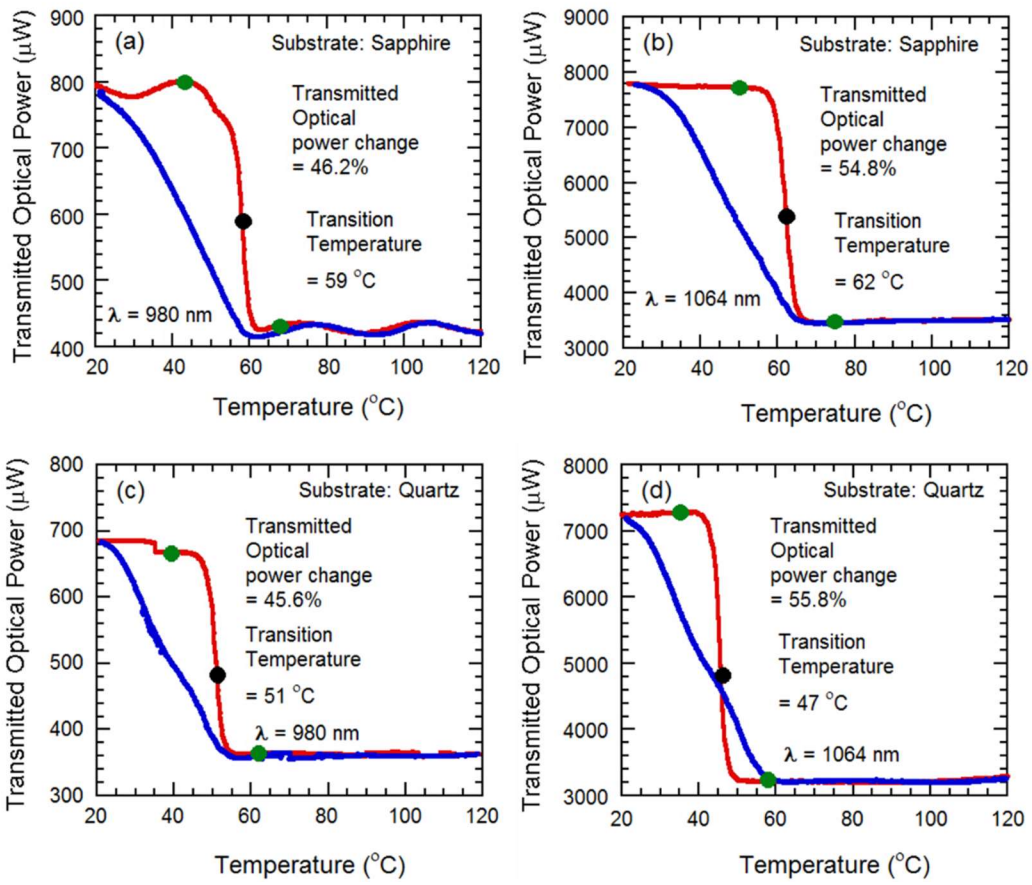

Figure 3.6: Transmitted optical power for two laser wavelengths (980 and 1064 nm), plotted against temperature, for the VO_2 thin films grown on c-plane sapphire (a, b), and AT-cut quartz (c, d), as they undergo metal-insulator transition (SMT). The transmitted optical power change, along with the beginning (green dots), mid (black dots, corresponding to maximum slope points in the curves), and end transition temperatures (green dots) are shown for all the samples.

Comparing the electrical and the optical transition plots in Figs. 3.4 and 3.6 for AT-cut quartz and c-plane sapphire substrates, we find that the forward optical transitions are much sharper, with significantly lower transition temperatures, compared to those of the electrical transitions. This is likely due to the fact that the electrical transition plots are influenced by the resistance of almost the entire VO_2 film, which changes temperature due to the thermal energy provided by the heater through a comparatively slow process.

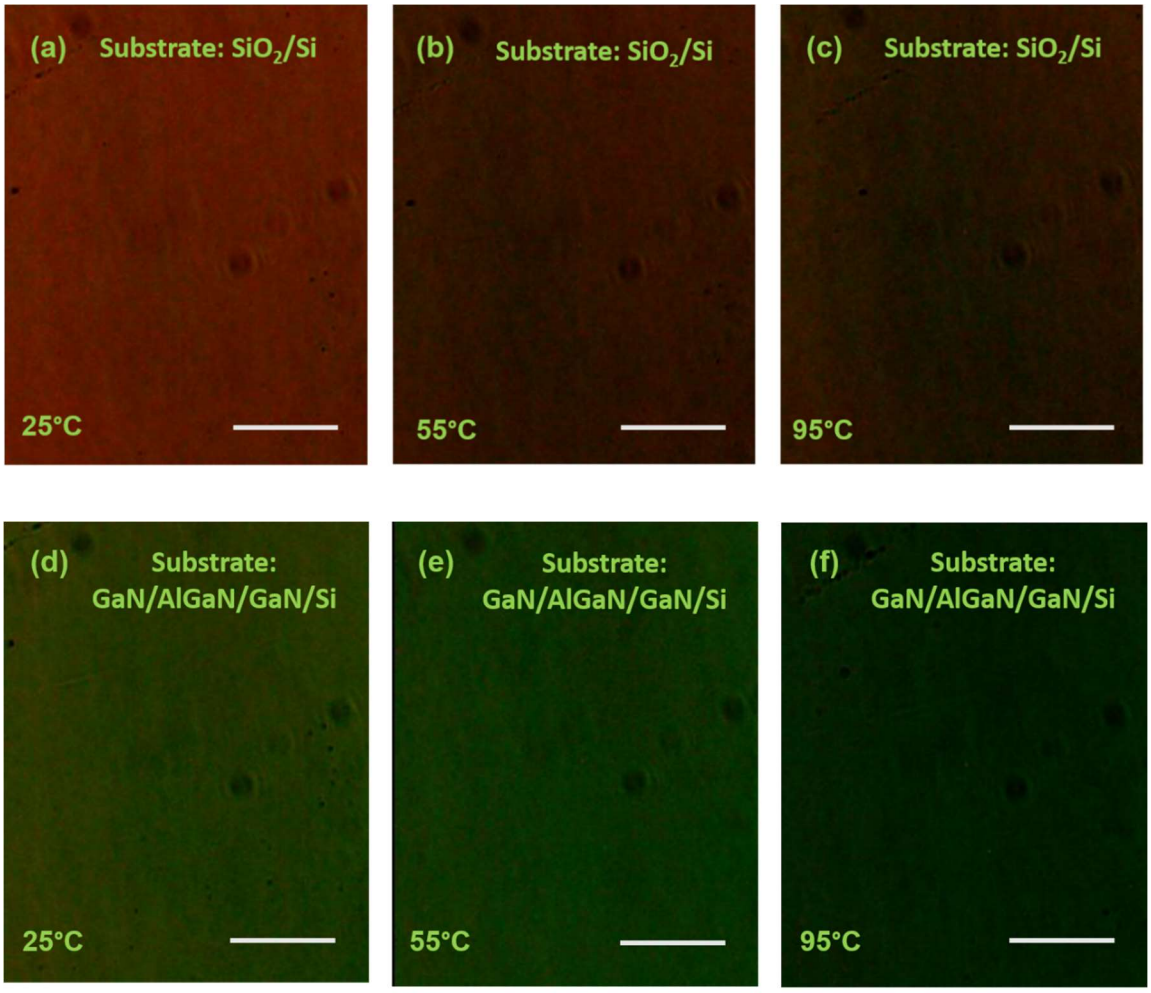

Figure 3.7: Optical microscopy images (20 × magnification) of VO_2 thin films (5 × 3 mm) grown on SiO_2/Si substrate (a, b, c) and GaN/AlGaN/GaN/Si substrate (d, e, f) taken near the beginning (25°C), at the middle (55°C), and toward the end (95°C) of the metal-insulator transition (SMT). As the samples undergo phase transition, their color changes significantly from lighter to darker. The scale bar: 200 µm for all substrates

On the other hand, during optical transition, the transmitted optical power is influenced only by the small area of the VO_2 film on which the laser is focused. Since the transition of that small area is affected both by the thermal energy provided by the heater and the energy absorbed from the laser power focused on it, the transition happens much quicker,

Table 3.1: Summary of the material, electrical and optical properties of the films synthesized on the four different substrates Sapphire, SiO_2/Si, AT-cut quartz, and GaN/AlGaN/GaN/Si

Parameters	c-plane Sapphire	SiO_2/Si	AT-cut Quartz	GaN/AlGaN/GaN/Si
rms roughness (nm)	8.19	7.37	10.3	9.75
2θ angles of prominent XRD peaks (FWHM)	38.36° (020) (0.14°)	69.28° (202) (0.06°)	38.5° (020) (0.20°)	38.52° (020) (0.16°)
2θ angles of common XRD peaks (FWHM)	38.36° (020) (0.14°)	38.42° (202) (0.16°)	38.5° (020) (0.20°)	38.52° (020) (0.16°)
Electrical Transition temperature (forward)	70 °C	75 °C	63 °C	63°C
Electrical Transition temperature (reverse)	65 °C	69 °C	59 °C	65°C
Optical Transition temperature at λ = 1064 nm	62 °C	-	47°C	-
Resistance transition ratio	1094	1065	1017	665
Activation energy at semiconducting phase (eV)	0.277	0.134	0.252	0.259
Activation energy at metallic phase (eV)	0.079	0.061	0.067	0.062

Change of Transmitted laser power or color at λ = 980 nm (%)	46.2	Brown to brownish-green	45.6	Lighter to darker green
Change of Transmitted laser power or color at λ = 1064 nm (%)	54.8	Brown to brownish-green	55.8	Lighter to darker green

which is manifested as a much steeper transition slope and significantly reduced transition temperature.

The VO_2 on SiO_2/Si and GaN/AlGaN/GaN/Si did not allow any transmission of laser power in the near IR region, as the silicon substrate absorbed all the light from the laser (VO_2 on Si only partially allows transmission of laser at mid IR wavelengths i.e. ~2500 nm, still significantly reducing the optical transmitted power by 55%) [40].

However, we recorded the significant color change (from optical microscopy images) of the VO_2 thin films (from lighter to darker) while undergoing the SMT, which is consistent with earlier reports [22]. Optical images of the VO_2 thin films, (a) near the beginning (25°C), (b) middle (55°C), and (c) toward the end (95°C) of the SMT, are shown in Fig. 3.7, which indicates significant darkening of the film as higher temperatures.

Table 3.2: Summary of the transition temperature and resistance ratio reported for VO_2 films on various substrates synthesized by multiple methods

Substrate	Reference	Synthesis process	Film thickness (nm)	Transition temperature (°C)	Resistance ratio	Crystal type
Sapphire	Zhao et al. [26]	DC reactive spluttering	120	65	48000	Monocrystalline
	Yu et al. [42]	DC magnetron sputtering	120	80	1300	Amorphous
	Jian et al. [43]	Pulsed laser deposition	30	48	7200	Monocrystalline
	Bian et al. [44]	Pulsed laser deposition	200	46		Polycrystalline
	Kovacs et al. [45]	Pulsed laser deposition	28		2000	Polycrystalline
	Yang et al. [46]	Pulsed laser deposition	200	75	15000	Dual orientation
	Chae et al. [47]	Laser ablation	-	65	18000	Monocrystalline
	This paper	**Direct oxidation**	**140**	**68**	**1094**	**Polycrystalline**
SiO_2/Si	Kovacs et al. [45]	Pulsed laser deposition	36	55	100	Polycrystalline
	Chae et al. [47]	Laser ablation	-	65	10	Polycrystalline
	Bhardwaj et al. [48]	Reactive pulsed laser deposition	-	55	100	Polycrystalline
	Youn et al. [49]	Pulsed laser ablation	90	68	50	Polycrystalline
	This paper	**Direct oxidation**	**140**	**72**	**1065**	**Polycrystalline**

Quartz	Liu et al. [12]	Aqueous sol-gel process	400	68	500	Polycrystalline
	Zhang et al. [40]	RF plasma assisted O-MBE	60	85	400	Polycrystalline
	Dejene et al. [50]	Reactive Pulsed laser ablation	500	50	1000	Polycrystalline
	Kizuka et al. [51]	Reactive RF magnetron sputtering	300	59	1188	Polycrystalline
	Dang et al. [52]	Reactive RF magnetron sputtering	300	67	105	Polycrystalline
	Taha et al. [53]	Pulsed DC magnetron sputtering	150	73	300	Crystalline
	Liu et al. [54]	Reactive Pulsed laser ablation		59	2000	Amorphous
	This paper	**Direct oxidation**	**140**	**61**	**1017**	**Polycrystalline**
III-Nitrides	Singh et al. [35]	Low pressure CVD		65	300	Polycrystalline
	Slusar et al. [38]	Pulsed laser deposition	130	77	1000	Monocrystalline
	This paper	**Direct oxidation**	**140**	**64**	**665**	**Polycrystalline**

This can be attributed to lower reflection of light as more of it absorbed in the material, which behaves like a lossy medium for the EM waves [41]. Comparison with other reports are shown in Table 3.3.

Effect of vanadium thickness on electrical and optical properties of VO_2/quartz:

In the system of VO_2 synthesis by direct oxidation, a vital step is deposition of vanadium metal on the substrate by electron beam evaporation. We can select the thickness of vanadium metal film prior to deposition. We wanted to observe if different thicknesses of vanadium have any significant effect on the substrate. Resistance change of VO_2 due to semiconductor to metal transition VO_2 characteristics later on. We found out that the effect is quite significant and drastic. The variation of metal thickness plays a highly important role not only on the VO_2 characteristics, but also the synthesis parameters

Table 3.3: Comparison of the synthesis parameters for samples grown on Quartz substrates (Deposited Vanadium of three different thicknesses)

V thickness	**35 nm**	**55 nm**	**70 nm**
Chamber pressure	164 mTorrs	224 mTorrs	227 mTorrs
Reaction Temperature	485°C	485°C	485°C
Gas Flow ratio N_2 : O_2	300 sccm : 75 sccm	300 sccm : 75 sccm	300 sccm : 75 sccm
Oxidation duration	8 minutes	15 minutes	25 minutes

For the AT-cut quartz substrate, we have optimized the synthesis parameters for three different thicknesses of vanadium metal film (35 nm, 55 nm and 70 nm). It should be

noted that deviation from these optimized parameters will cause the vanadium metal to be over-oxidized or under-oxidized, which is not desirable for growing a good quality of vanadium thin film. Usually, the higher thickness of vanadium film requires higher amount of duration of oxidation.

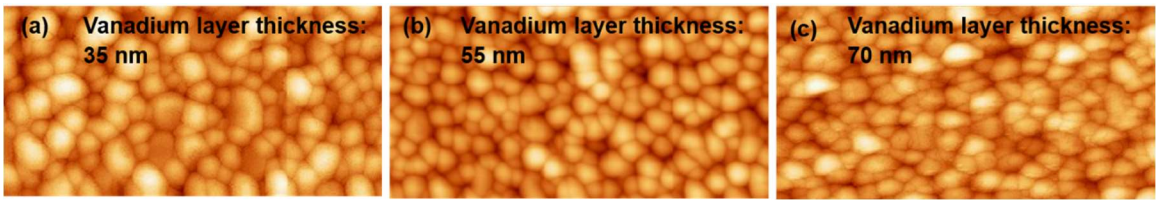

Figure 3.8: Surface morphology images (5 × 2.5 μm) of thin films synthesized from (a) 35 nm Vanadium (b) 55 nm Vanadium (c) 70 nm Vanadium deposited on AT-cut quartz

However, we recorded the significant color change (from optical microscopy images) of the VO_2 thin films (from lighter to darker) while undergoing the SMT, which is consistent with earlier reports [22]. AFM images of the VO_2 thin films, (a) near the beginning (25°C), (b) middle (55°C), and (c) toward the end (95°C) of the SMT, are shown in Fig. 3.8, which indicates significant darkening of the film as higher temperatures. For the analyzing the surface morphology, we performed atomic force microscopy (AFM) in tapping mode on all three thickness variations of VO_2/quartz and determine the rms roughness. The lattice structure of the VO_2 films were analyzed by x-ray diffraction patterns as before, using Cu Kα radiation, recording the diffracted beam from 5° to 90° with a step size of 0.02°. All the thin films show common XRD peak at

VO_2 (011) plane, with FWHM ranging from 0.10° to 0.14°, as we see in food. The XRD pattern validates the significance presence of decent quality polycrystalline VO_2 (011) thin film by analyzing its diffraction beam angle, peak intensity and full width half max.

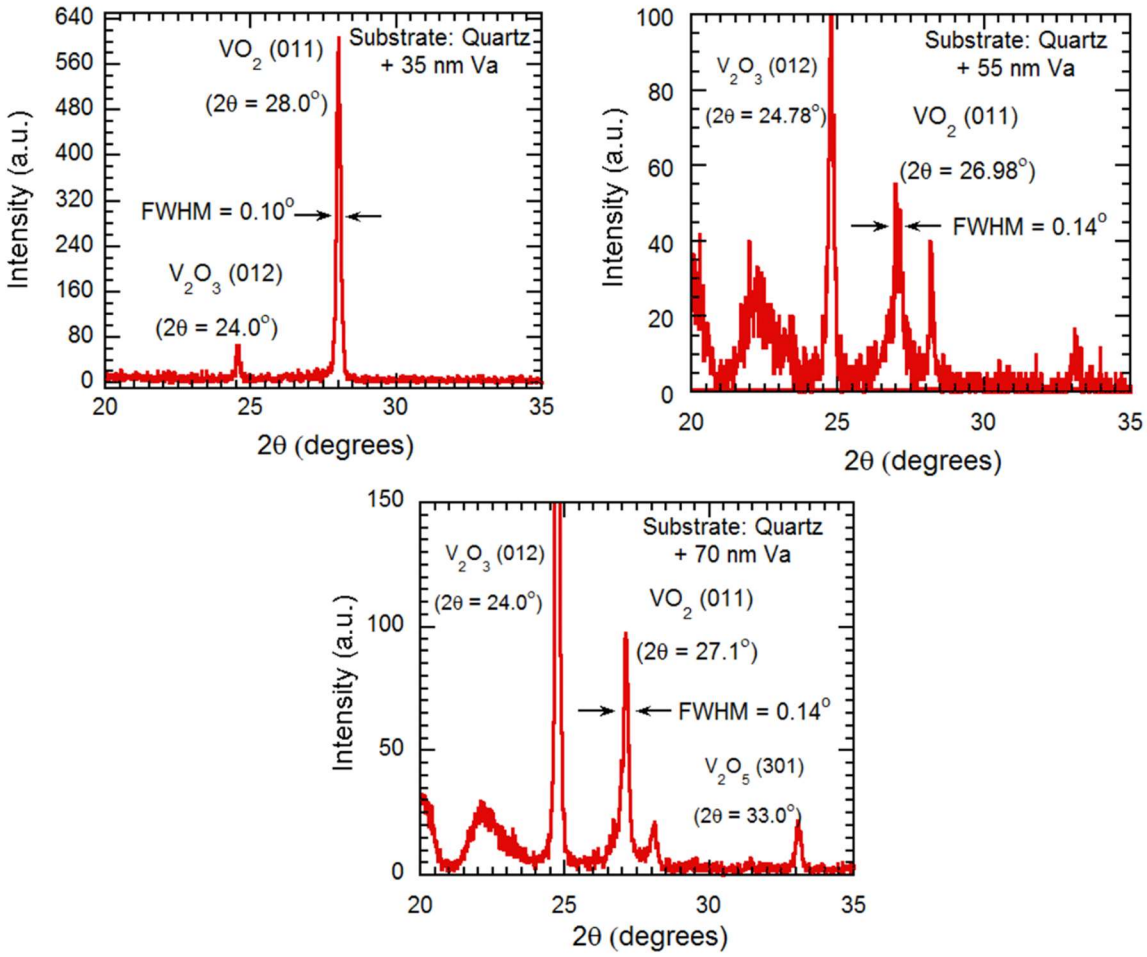

Figure 3.9: X-ray diffraction peaks are presented for the VO_2 thin films synthesized on AT-cut quartz with deposited vanadium thickness (a) 35 nm, (b) 55 nm, (c) 70 nm. The VO_2 (011) along with their respective full width at half maxima (FWHM), are pointed out with arrows.

The optimization of synthesis parameters has ensured good quality of polycrystalline VO_2 thin film with different thicknesses (35 nm, 55 nm and 70 nm), as we

saw from the AFM images and rms roughness, and XRD patterns. Using the experimental setup shown in Fig. 2.2, we observe the resistance changes with temperature variation when heat is applied, due to the semiconductor to metal transition, and plotted in a semi-logarithmic scale. The ratio of resistance at semiconductor phase and metallic phase is calculated for all three types samples, and we find them in same order and range (821, 860 and 846), as shown in Fig. 3.10.

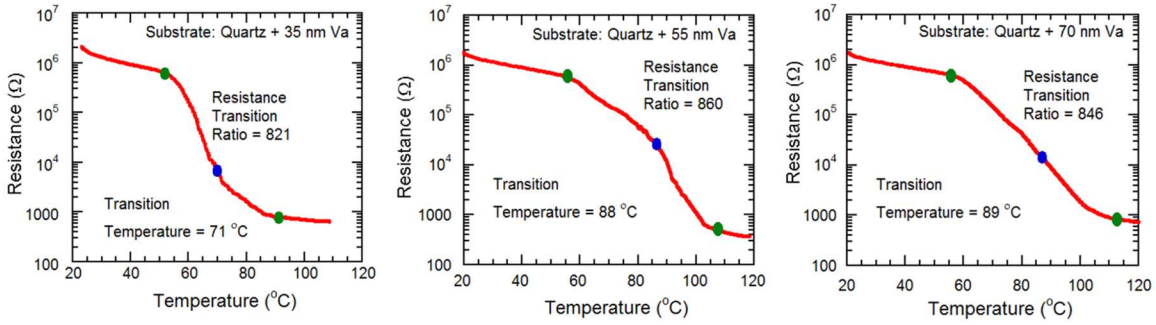

Figure 3.10: Semi-log plots of resistivity variation as a function of temperature for the VO_2 thin films grown on AT-cut quartz with deposited vanadium thickness (a) 35 nm, (b) 55 nm, (c) 70 nm as they undergo semiconductor-metal transition (SMT). The transition resistance ratios, along with the beginning (green dots), mid (blue dots, corresponding to maximum slope points in the curves), and end transition temperatures (green dots) are shown for all the samples

Two wavelengths of IR laser (980 nm and 1064 nm) are transmitted through the three thicknesses of VO_2/quartz thin films. The transmitted optical power is measured with a photodetector and power meter similar to the Fig. 2.2. The temperature is varied by applying heat and the transmitted optical power exhibits a sharp decrease during the semiconductor to metal transition of the VO_2 film. At each wavelength, we observe the change of transmitted power increases due to the increase of vanadium thickness prior to the VO_2 synthesis.

Table 3.4: Comparison of the results of electrical and optical characterization for samples grown on Quartz substrates (Deposited Vanadium of three different thicknesses)

V thickness		**35 nm**	**55 nm**	**70 nm**
Resistance transition ratio		821	872	846
RMS roughness (nm)		15.7	7.6	12.5
2θ angles of common XRD peaks (FWHM)		28° (011) (0.10°)	26.98° (011) (0.14°)	27.1 (011) (0.14°)
Transmitted power change	λ = 980 nm	34.6 %	42.1 %	47.7 %
	λ = 1064 nm	39.4 %	54.5 %	60.2 %

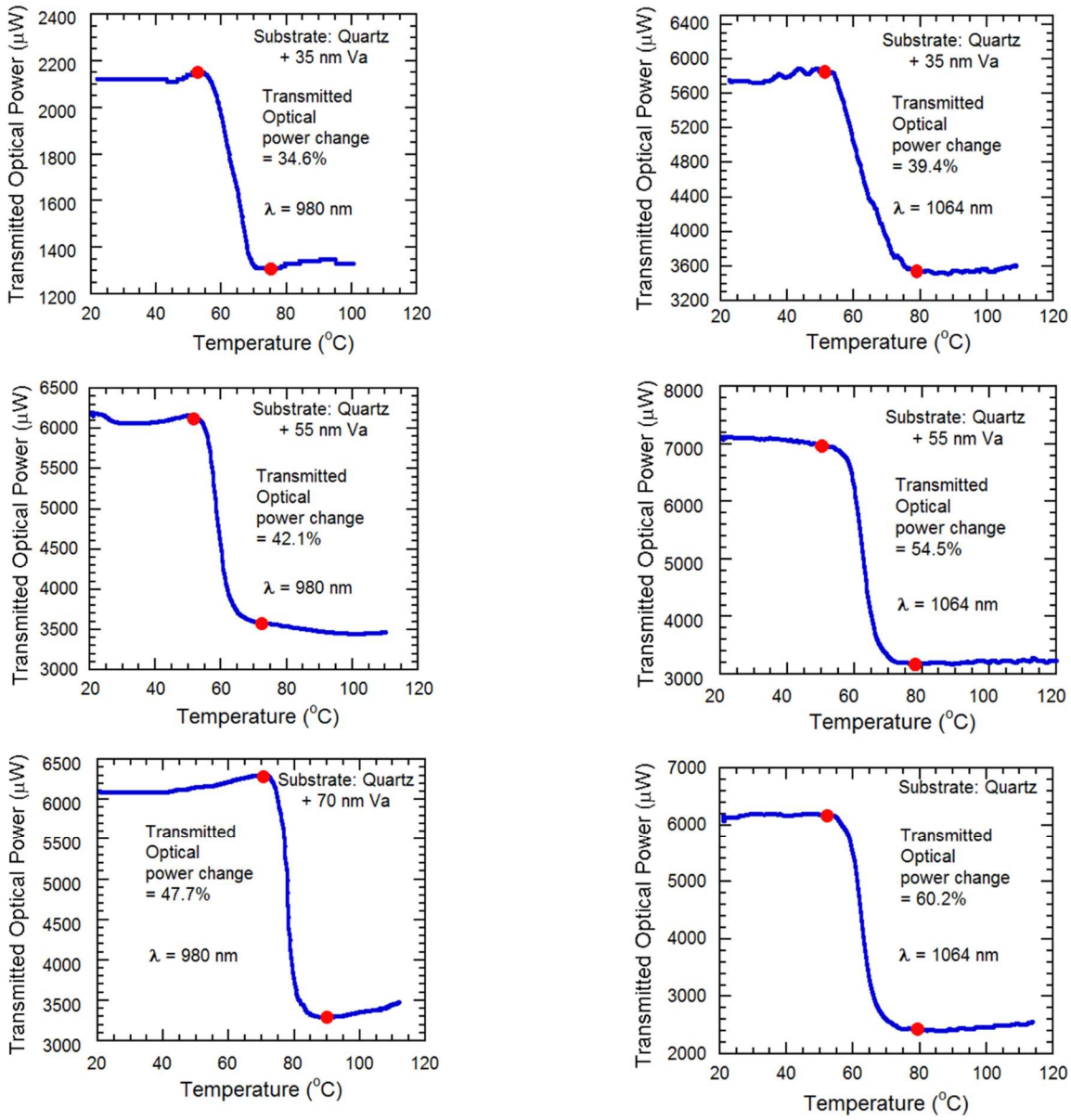

Figure 3.11: Transmitted optical power for two laser wavelengths (980 and 1064 nm), plotted against temperature, for the VO_2 thin films grown on AT-cut quartz, with deposited vanadium thickness (a, d) 35 nm, (b, e) 55 nm, (c, f) 70 nm as they undergo metal-insulator transition (SMT). The transmitted optical power change, along with the beginning and end (red dots), corresponding to beginning and end transition temperatures are shown for all the samples.

CHAPTER FOUR

CONCLUSION

In conclusion, we have reported on the synthesis of high quality VO_2 films using direct oxidation method, on two piezoelectric substrates, and compared them to the films grown on two traditional non-piezoelectric substrates, SiO_2/Si and sapphire. Structural, electrical and optical characterization of the VO_2 films underline their high quality that is quite comparable to the best results on films synthesized by other techniques on various substrates. The VO_2 films synthesized on both piezoelectric GaN/AlGaN/GaN/Si and AT-cut quartz substrates exhibiting excellent crystalline, morphological and electrical properties, with demonstration of a high resistivity transition ratio and very high transmitted optical power change caused by SMT. We had to select the most feasible technique for VO_2 thin film growth, optimizing the parameters, Triggering and analyzing the change of characteristics due to SMT. VO_2 is selected because of its easiness to synthesize and characterize, and its easily observable SMT properties. The sharp transition in electrical and structural properties of Vanadium dioxide during the Metal-Insulator Transition (MIT) is highly attractive for various electronic, optoelectronic and sensing applications. In this work, we have optimized direct oxidation method for VO_2 thin film synthesis and implemented it to grow high quality polycrystalline VO_2 thin films on piezoelectric substrates (AT-cut quartz and GaN/AlGaN/GaN/Si) and compared them with non-piezoelectric substrates (c-plane sapphire and SiO_2/Si). Vanadium metal films were deposited on the substrates by electron beam evaporation and oxidized in our low pressure system at a critical reaction temperature, with an optimized mixture of high

purity gases at a very low chamber pressure. The oxidation duration, cooling condition and duration and substrate orientation play a crucial role for synthesis of high quality VO_2 films. The substrate was chosen as both large surface area and small patterned surface area. Material characterization was performed on the VO_2 films by atomic force microscopy and x-ray diffraction to determine their surface and structural quality. The synthesized polycrystalline VO_2 films were etched by Bosch process from the bottom of the surface to release membrane-like structure for strain based sensing applications. Also they were patterned in the top surface by depositing metal contacts to create finger patterned VO_2 structure, which will pave the way for fabricating surface acoustic wave generating devices.

The electrical characterization of the grown VO_2 films provided resistivity transition ratio by a huge magnitude, at the typical expected critical temperature when the SMT takes place. The sharpness and smoothness of the resistivity vs. temperature plots indicate the well uniformed growth of the VO_2 film, and the high intensity peaks with low FWHM indicates the excellent crystal quality of the polycrystalline films, almost as good as the monocrystalline films. The high percentage of reduction of IR wavelength transmission through our VO_2 films indicated future promising applications of our VO_2 films.

Future work:

The SMT of the our VO_2 films are triggered by applying heat, but they can be triggered by electric field and laser heating and mechanical strain as well. The SMT induction by electric field removes the necessity of extra heating to use the VO_2 film in switching applications. When the applied electric field crosses the threshold field, the VO_2 undergoes SMT, shifts its phase and turn on or off the switch as it is designed. Periodic electric field into a VO_2 with finger pattern on a piezoelectric substrate can generate surface acoustic waves on the surface. This acoustic waves can create periodic mechanical strain on the VO_2 film, which can induce phase transition in a periodic fashion.

We are also planning to use VO_2 film as optical chopper or modulator. Allowing a continuous IR beam through the VO_2 and applying a periodic voltage on the VO_2 with finger pattern can induce SMT in the VO_2 in a periodic manner. The continuous IR beam will experience the semiconducting and metallic VO_2 in a periodic manner, which will make the transmission through the film periodically high and low. We can control the input voltage frequency and trigger the SMT in the VO_2 according to our choice, leading to the VO_2 film being a fast and robust optical modulator.

We are also planning to design and fabricate microcantilever structure coated with VO_2 thin film. In a vacuum environment, the cantilevers can be deflected very easily and make them experience mechanical strain. This strain can induce SMT in the VO_2 film on

the cantilever, and can be used as a fast switch for turning on or off a microtransistor designed on the mesa of the cantilevers.

It is in our agenda to induce SMT by a high powered laser. Instead of applying heat with the ceramic heater used in this research, which heats the whole VO_2 film and impossible to control and contain the heat spatially and periodically, the high powered laser comes to rescue. The high powered laser focuses on a quite small area of the VO_2 film surface, thus allowing us to select and decide which portion of the surface we want to induce SMT. Also, we can apply periodic pulse to the laser, allowing it to be on or off periodically at any frequency, and consequently allowing the laser pointed area of the VO_2 surface to undergo SMT periodically.

We have observed that metal doped VO_2 has a much lower transition temperature rather than the undoped VO_2. This can enable us to synthesize VO_2 film with appropriate amount of metal doping so that the transition temperature is as close as the room temperature. This will lead to fabrication of highly sensitive thermal sensor, which can undergo SMT at a quite low temperature and provide high precision temperature detection.

Undoubtedly, VO_2 is a highly promising material with a new unexplored realm of possibilities. If we are successful to meet all our research agenda described above, we can guarantee that it will lead to a revolution in semiconductor based sensing industry.

REFERENCES

[1] L. L. Fan, S. Chen, Y. F. Wu, F. H. Chen, W. S. Chu, X. Chen, C. W. Zou, and Z. Y. Wu, Growth and phase transition characteristics of pure M-phase VO_2 epitaxial film prepared by oxide molecular beam epitaxy, Applied Physics Letter, vol. 103, no. 131914, 1-6 (2013).

[2] M. A. Baqir, and P. K. Choudhury, On the VO_2 metasurface-based temperature sensor, Journal of the Optical Society of America, vol. 36, no. 8, F123-F130 (2019).

[3] Y. Cui, Y. Ke, C. Liu, Z. Chen, N. Wang, L. Zhang, Y. Zhou, S. Wang, Y. Gao, and Y. Long, Thermochromic VO_2 for energy-efficient smart windows, Joule Cellpress Reviews, 1707-1746 (2018).

[4] J. Lee, D. Lee, S. J. Cho, J. –H. Seo, D. Liu, C. –B. Eom, and Z. Ma, Epitaxial VO_2 thin film-based radio-frequency switches with thermal activation, Applied Physics Letter, vol. 111, no. 063110, 1-5 (2017).

[5] D. Torres, T. Wang, J. Zhang, X. Zhang, S. Dooley, X. Tan, H. Xie, and N. Sepúlveda, VO_2-based MEMS mirrors, Journal of Microelectromechanical Systems, vol. 25, no. 4, 780-787 (2016).

[6] D. Gajula, F. Bayram, I. Jahangir, D. Khan, and G. Koley, Dynamic response of VO_2 mesa based GaN microcantilevers for sensing applications, Proc. IEEE Sensors (2019).

[7] C. Piccirillo, R. Binions, and I. P. Parkin, Synthesis and functional properties of vanadium oxides: V_2O_3, VO_2, and V_2O_5 deposited on glass by aerosol-assisted CVD, Chemical Vapor Deposition vol. 13, 145-151 (2007).

[8] L. Kang, Y. Gao, H. Luo, A novel solution process for the synthesis of VO_2 thin films with excellent thermochromic properties, Applied Materials and Interfaces, vol. 1, no. 10, 2211-2218 (2001).

[9] C. Zhang, C. Koughia, O. Günes, J. Luo, N. Hossain, Y. Li, X. Cui, S. –J. Wen, R. Wong, Q. Yang, and S. Kasap, Synthesis, structure and optical properties of high-quality VO_2 thin films grown on silicon, quartz and sapphire substrates by high temperature magnetron sputtering: Properties through the transition temperature, Journal of Alloys and Compounds, 848, 156323 (1-13) (2020).

[10] Ch. V. R. Reddy, E. H. Walker Jr, S. A. Wicker, Q. L. Williams, R. R. Kaluru, Synthesis of VO_2 (B) nanorods for Li battery application, Current Applied Physics, vol. 9, 1195-1198 (2009).

[11] M. J. Powell, I. J. Godfrey, R. Queseda-Cabrera, Qualitative XANES and XPS analysis of substrate effects in VO_2 thin films: A route to improving chemical vapor deposition synthetic methods? The Journal of Physical Chemistry, vol. 121, 20345-20352 (2017).

[12] D. –Q. Liu, W. –W. Zheng, H. –F. Cheng, and H. –T. Liu, Thermochromic VO2 thin film prepared by post annealing treatment of V_2O_5 thin film, Advanced Materials Research, 79-82, 747-750 (2009).

[13] O. A. Novodvorsky, L. S. Parshina, and O. D. Karamova, Influence of the conditions of pulsed laser deposition on the structural, electrical, and optical properties of VO_2 thin films, Bulletin of the Russian Academy of Sciences, vol. 80, no. 4, 376-380 (2016).

[14] B. Guo, D. Wan, A. Ishaq, H. Luo, and Y. Gao, Direct synthesis of high-performance thermal sensitive VO_2 (B) thin film by chemical vapor deposition for using in uncooled infrared detectors, Journal of Alloys and Compounds, vol. 715, 129-136 (2017).

[15] J. Vlček, D. Kolenatý, J. Houška, T. Kozák and R Čerstvý, Controlled reactive HiPIMS—effective technique for low-temperature (300 °C) synthesis of VO_2 films with semiconductor-to-metal transition, Journal of Physics D: Applied Physics, vol. 50, no. 38, 1-7

[16] J. Houska, D. Kolenaty, J. Vlcek, and R. Cerstvy, Properties of thermochromic VO_2 films prepared by HiPIMS onto unbiased amorphous glass substrates at a low temperature of 300 °C, Thin Solid Films, vol. 660, 463-470 (2018).

[17] J. Houska, D. Kolenaty, J. Vlcek, T. Barta, J. Rezek, and R. Cerstvy, Significant improvement of the performance of $ZrO_2/V_{1-x}W_xO_2/ZrO_2$ thermochromic coatings by utilizing a second-order interference, Solar Energy Materials and Solar Cells, vol. 191, 365-371 (2019).

[18] D. Kolenatý, J. Vlček, T. Bárta, J. Rezek, J. Houška and S. Haviar, High-performance thermochromic VO_2-base coatings with a low transition temperature deposited on glass by a scalable technique, Scientific Reports, vol. 10, no. 11107, 1-12 (2020).

[19] S. Chen, J. Lai, J. Dai, H. Ma, H. Wang, and X. Yi, Characterization of nanostructured VO_2 thin films grown by magnetron controlled sputtering deposition and post annealing method, Optics Express, vol. 17, no. 26, 24153-24161 (2009).

[20] D. Li, M. Li, J. Pan, Y. X. Zhang, and G. H. Li, Thermal Oxidation of V_2O_3 Nanocrystals: A Template Method for the Fabrication of Monoclinic Phase VO_2 Nanocrystals, Journal of Nanoscience and Nanotechnology, vol. 13, 5469-5473 (2013).

[21] X. Liu, R. Ji, Y. Zhang, H. Li, and S. –W. Wang, Annealing process and mechanism of glass based VO_2 film from V oxidation in pure oxygen atmosphere, Optical and Quantum Electronics, 48, article 453, 1-10 (2016).

[22] L. Rongrong, H. Peng, H. Wanxia, Y. Jiazhen, and C. Jinghan, Optical switching and color changing properties of VO_2 films on muscovite substrate, Rare Metal Materials and Engineering, vol. 41, issue 8, 1327-1330 (2012).

[23] R. Lindstrom, V. Maurice, S. Zanna, L. Klein, H. Grault, L. Perrigaud, C. Cohen and P. Marcus, Thin films of vanadium oxide grown on vanadium metal: oxidation conditions to produce V_2O_5 films for Li-intercalation applications and characterization by XPS, AFM, RBS/NRA, Surface and Interface Analysis, vol. 38, 6-18 (2006).

[24] T. Lin, J. Wang, G. Liu, L. Wang, X. Wang and Y. Zhang, influence of discharge current on phase transition properties of high quality polycrystalline VO_2 thin film fabricated by HiPIMS, Materials, vol. 10, no. 633, 1-12 (2017).

[25] M. R. Bayati, R. Molaei, F. Wub, J. D. Budai, Y. Liu, R. J. Narayan and J. Narayan, Correlation between structure and semiconductor-to-metal transition characteristics of VO_2/TiO_2/sapphire thin film heterostructures, Acta Materialia, vol. 61, 7805-7815 (2013).

[26] Y. Zhao, J. H. Lee, Y. Zhu, M. Nazari, C. Chen, H. Wang, A. Bernussi, M. Holtz, and Z. Fan, Structural, electrical, and terahertz transmission properties of VO_2 thin films grown on c-, r-, and m-plane sapphire substrates, Journal of Applied Physics, vol. 111, 053533 (2012).

[27] P. Markov, R. E. Marvel, H. J. Conley, K. J. Miller, R. F. Haglund Jr., and S. M. Weiss, Optically monitored electrical switching in VO_2, ACS Photonics, 2, 1175-1182 (2015).

[28] Z. Yang, C. Ko, and S. Ramanathan, Metal-insulator transition characteristics of VO_2 thin films grown on Ge (100) single crystals, Journal of Applied Physics, 108, 07308 (1-7) 2010.

[29] S. Rathi, J. –H. Park, In. –y. Lee, J. M. Baik, K. S. Yi, and G. –H. Kim, Unravelling the switching mechanisms in electric field induced insulator–metal transitions in VO_2 nanobeams, Journal of Physics D: Applied Physics, 47, 295101 (1-9) (2014).

[30] L. Q. Mai, B. Hu, T. Hu, W. Chen, and E. D. Gu, Electrical property of Mo-doped VO_2 nanowire array film by melting-quenching sol-gel method, The Journal of Physical Chemistry B, 110, 19083-19086 (2006)

[31] C. Chen, Y. Zhao, X. Pan, V. Kuryatkov, A. Bernussi, M. Holtz, and Z. Fan, Influence of defects on structural and electrical properties of VO_2 thin films, Journal of Applied Physics, 110, 023707 (1-7) (2011).

[32] C. N. Berglund, and H. J. Guggenheim, Electronic properties of VO_2 near semiconductor-metal transition, Physical Review, Bell Telephone Laboratories, vol. 185, no. 3, 1022-1033 (1969).

[33] J. Wei, Z. Wang, W. Chen and D. H. Cobden, New aspects of the metal–insulator transition in single-domain vanadium dioxide nanobeams, Nature Technology, vol. 4, 420-424 (2009).

[34] S. Kumar, J. P. Strachan, M. D. Pickett, A. Bratkovsky, Y. Nishi, and R. S. Williams, Sequential electronic and structural transitions in VO_2 observed using x-ray absorption spectromicroscopy, Advanced Materials, 26, 7505-7509 (2014).

[35] R. T. Singh, D. Khan, D. Gajula, F. Bayram, and G. Koley, Synthesis and characterization of VO_2 on III nitride thin films using low pressure chemical vapor deposition for sensing applications, Proceedings of IEEE 13th Nanotechnology Materials and Devices Conference, 1-4 (2018).

[36] S. Azad, R. Singh, M. Munna, F. Bayram, D. Khan, H. Li, and G. Koley, Investigation of VO_2 thin film grown on III-nitride epitaxial layer, Proceedings of IEEE Nano 2020, 315-318 (2020).

[37] M. Qazi, III-V nitride based piezoresistive microcantilever for sensing applications, Applied Physics Letter, vol. 99, 99–103 (2011).

[38] T. Slusar, J.–C. Cho, B.–J. Kim, S. J. Yun, and H.–T. Kim, Epitaxial growth of higher transition temperature VO_2 films on AlN/Si, Applied Physics Letters Materials, vol. 4, 026101, 1-8 (2016).

[39] H. Harima, Properties of GaN and related compounds studied by means of Raman scattering, Journal of Physics: Condensed Matters, vol. 14, 967-993 (2002).

[40] D. Zhang, H.–J. Sun, M.–H. Wang, L.–H. Miao, H.–Z. Liu, Y.–Z. Zhang, and J. M. Bian, VO_2 thermochromic films on quartz glass substrate grown by RF-plasma-assisted oxide molecular beam epitaxy, Materials, 10, 3174 (1-10) (2017).

[41] Joushaghani, J. Jeong, S. Paradis, D. Alain, Wavelength-size hybrid Si-VO_2 waveguide electroabsorption optical switches and photodetectors, Optics Express, vol. 23, no. 3 (2015).

[42] S. Yu, S. Wang, M. Lu, and Lei Zuo, A metal-insulator transition study of VO_2 thin films grown on sapphire substrates, Journal of Applied Physics, vol. 122, no. 235102, 1-6 (2017).

[43] J. Jian, X. Wang, L. Li, M. Fan, W. Zhang, J. Huang, Z. Qi, and H. Wang, Continuous tuning of phase transition temperature in VO_2 thin films on c-cut sapphire substrates via strain variation, Applied Materials and Interfaces, vol. 9, no. 6, 5319-5327 (2017).

[44] J. Bian, L. Miao, S. Zhao, X. Li, C. Zou, D. Zhang, and Y. Zhang, Vanadium oxide films deposited on sapphire substrate with in situ AlN stress layer: structural, electric, and optical properties, Journal of Material Science, vol. 50, 5709-5714 (2015).

[45] G. J. Kovács, D. Bürger, I. Skorupa, H. Reuther, R. Heller, and H. Schmidt, Effect of the substrate on the insulator–metal transition of vanadium dioxide films, Journal of Applied Physics, vol. 109, no. 063708, 1-6 (2011).

[46] T. –H. Yang, R. Aggarwal, A. Gupta, H. Zhou, R. J. Narayan, and J. Narayan, Semiconductor-metal transition characteristics of VO_2 thin films grown on c- and r- sapphire substrates, Journal of Applied Physics, vol. 107, no. 053514, 1-7 (2010).

[47] B. G. Chae, D. H. Youn, H. T. Kim, S. L. Maeng, and K. Y. Kang, Fabrication and electrical properties of pure VO_2 phase films, Journal of the Korean Physical Society, vol. 44, no. 4, 884-888 (2004).

[48] D. Bhardwaj, A. Goswami, and A. M. Umarji, Synthesis of phase pure vanadium dioxide (VO_2) thin film by reactive pulsed laser deposition, Journal of Applied Physics, vol. 124, no. 135301, 1-7 (2018).

[49] D. –H. Youn, J. –W. Lee, B. –G. Chae, H. –T. Kim, S. –L. Maeng, and K. –Y. Kang, Growth optimization and electrical characteristics of VO_2 films on SiO_2/Si amorphous substrates, Journal of Applied Physics, vol. 95, no. 1407, 1-6 (2004).

[50] F. B. Dejene, and R.O. Ocaya, Electrical, optical and structural properties of pure and gold-coated VO_2 thin films on quartz substrate, Current Applied Physics, vol. 10, 508-512 (2010).

[51] H. Kizuka, T. Yagi, J. Jia, Y. Yamashita, S. Nakamura, N. Taketoshi, and Y. Shigesato, Temperature dependence of thermal conductivity of VO_2 thin films across metal–insulator transition, Japanese Journal of Applied Physics, vol. 54, no. 053201, 1-6 (2015).

[52] Y. Dang, D. Wang, X. Zhang, L. Ren, B. Li, and J. Liu, Structure and thermochromic properties of Mo-doped VO_2 thin films deposited by sol–gel method, Inorganic and Nano Metal Chemistry, vol. 49, no. 4, 120-125 (2019).

[53] M. Taha, S. Walia, T. Ahmed, D. Headland, W. Withayachumnankul, S. Sriram and M. Bhaskaran, Insulator–metal transition in substrate-independent VO_2 thin film for phase-change devices, Scientific Reports, vol. 7:178999, 1-10 (2017).

[54] D. –Q. Liu, C. Haifeng, Z. Wenwei, and Z. Chaoyang, Infrared thermochromic properties of VO_2 thin films prepared through aqueous sol-gel process, Journal of Wuhan University of Technology-Maters, vol. 10, no. 5, S61-S65 (2012).

[55] J. Ma, G. Xu, L. Miao, M. Tazawa, and S. Tanemura, Thickness-dependent structural and optical properties of VO_2 thin films, Japanese Journal of Applied Physics, vol. 50, 020215 (1-4) (2011).

[56] E. Radue, E. Crisman, L. Wang, S. Kittiwatanakul, and J. Lu, Effect of a substrate-induced microstructure on the optical properties of the insulator-metal transition temperature in VO_2 thin films, Journal of Applied Physics, vol. 113, 233104 (1-7) (2013).